C.P. No. 874

C.P. No. 874

LIBRARY
ROYAL AIRCRAFT ESTABLISHMENT
BEDFORD.

MINISTRY OF AVIATION

AERONAUTICAL RESEARCH COUNCIL

CURRENT PAPERS

Analysis of Hinge Moment Data for Rectangular and Near Rectangular Trailing Edge Controls at Supersonic and Transonic Speeds

by

D. Isaacs

LONDON: HER MAJESTY'S STATIONERY OFFICE

1966

PRICE 12*s* 0*d* NET

U.D.C. No. 533.694.511 : 533.6.013.155 : 533.6.011.35/5

C.P. No.874
May 1965

ANALYSIS OF HINGE MOMENT DATA FOR RECTANGULAR AND NEAR RECTANGULAR TRAILING EDGE CONTROLS AT SUPERSONIC AND TRANSONIC SPEEDS

by

D. Isaacs

SUMMARY

Similarity rules have been used at supersonic and transonic speeds to obtain a correlation of available experimental data on hinge moment curve slope, $(dC_H/d\eta)$, and to compare the experimental values with theoretical estimates.

The effects of varying control aspect ratio, thickness chord ratio, body interference, hinge line location, and trailing edge thickness are examined, suitable theoretical or empirical methods for predicting these effects are indicated, and their range of validity and accuracy determined.

Replaces R.A.E. Technical Report No.65105 - A.R.C. 27227.

CONTENTS

1 INTRODUCTION

A large amount of experimental data on trailing edge control hinge moments at supersonic and transonic speeds has accumulated during recent years. Although in several cases the individual experimental data have been compared with theoretical estimates, a much better understanding can often be obtained by a more comprehensive analysis covering a wider range of experimental configurations.

Using similarity parameters a correlation of the available experimental data is attempted here, and the effects of control aspect ratio, thickness chord ratio, body interference, hinge line location, and trailing edge thickness are examined.

At transonic speeds an approximate theory is developed for $dC_H/d\eta$ of a rectangular control, based on the transonic small perturbation theory solution for the flow over a two dimensional wing of double-wedge profile. A comparison is made between the experimental data and this theory at transonic speeds, and with existing linear theory at supersonic speeds, in order to determine the range of applicability of theoretical methods, and to obtain a method of extrapolating the data to configurations outside the range of existing measurements.

2 CHOICE OF DATA

A complete list of all configurations analysed in this report is given in Table 1. This shows in some detail all relevant geometrical properties of the wings and controls, in addition to giving the reference number of the data, the Reynolds number of the tests, and brief details of the experimental technique used.

Although some hinge moment measurements made on a free flight model have been included in the analysis, most of the data is of wind tunnel origin and includes measurements made using most of the standard testing techniques, viz. sting mounted models and half models mounted on reflection plates over the entire speed range, with the addition of the "transonic bump" technique[1] at transonic speeds.

In all cases the hinge moments have been measured directly using internal strain gauge balances located either in the wing along the hinge line, or alternatively, within the body of a wing-body combination, or beneath a reflection plate or bump surface.

Measurements of control hinge moments on a two-dimensional wing of circular-arc section by Czarnecki and Mueller[2], have shown the importance of fixing boundary layer transition at low Reynolds numbers at supersonic speeds. At a Reynolds number of 10^6 based on wing chord, transition did not occur naturally, and measured values of $dC_H/d\eta$ at zero η were much lower than those measured with transition artificially fixed. In view of this result, it would have been logical to select data for analysis where either boundary-layer transition had been artificially fixed, or alternatively, where the Reynolds number was sufficiently large for natural transition to have taken place ahead of the control. However, due to the small amount of data available, it has been necessary to include in the present analysis data which had been obtained under conditions of natural transition, with no record of where transition had occurred. Although some of these measurements with natural transition were obtained at Reynolds numbers (based on wing root chord) as low as 2.2×10^6, the majority of the results were obtained at Reynolds numbers of 5×10^6 and above.

Not all the available data has been included in the following analysis. Some showed large amounts of scatter between repeat tests on the same configuration, and was rejected on grounds of accuracy. Although controls of near rectangular planform have been included in the analysis, e.g. rectangular controls with raked tips, in some cases controls were considered to deviate too much from a rectangular shape and the data were not used. Similarly, data for controls having discontinuities in their profile shape (other than double-wedge profile) have been ignored. In some cases of rectangular controls the control geometry was so complicated that the data could not be conveniently analysed, e.g. the individual effects of aspect ratio, hinge line location, hinge line thickness, and trailing edge thickness could not be identified. In the case of outboard, part span controls on reflection plate mounted wings at transonic speeds, it was often difficult to determine the effect the reflection plate had on the control hinge moments, i.e. the control was neither so far away from the reflection plate that its effect could be ignored, nor was it so close to the reflection plate that the control aspect ratio was effectively doubled. In cases like this the data were rejected.

3 METHOD OF ANALYSIS OF DATA

The analysis was restricted to rectangular and near rectangular controls, with less than 10° of leading and trailing edge sweep (Fig. 1), and with the hinge line parallel or nearly parallel to the control leading edge.

The aspect ratio of the control was defined as

$$A = b^2/S ,$$

where b is the control span and S is the control area. In the case of a control mounted on a reflection plane or on an axis of symmetry of a circular cross section body, the aspect ratio of the control was assumed to be twice that of the exposed panel.

Fig.2 illustrates the definition of control span (b) used in the analysis. In the case of a control mounted on a body, a gross semi-span (s) which includes the body radius was defined,

$$s = \frac{b}{2} + r \ .$$

A control whose span is identical to the wing has 'free' tips or side edges, whereas a control whose span is less than that of the wing can have either 'free' tips or tips which are 'bounded' by the wing (Fig.2).

Details of wing and control section shape were given in the original data in most cases. However, additional information was required in the case of some NASA type aerofoils and this was obtained from reference 3. The majority of controls had a linear variation of thickness with chordwise location (Fig.3a and b), and the thickness chord ratio of the control did not vary across its span. In these cases the control thickness parameter τ was defined as

$$\tau = \frac{t}{c} \ ,$$

where t is the control thickness at its leading edge and c is the chord. For controls with plane upper and lower surfaces, the trailing edge included angle was defined as

$$\phi = 2 \tan^{-1} \frac{1}{2} (\tau - \tau_1) \ ,$$

or

$$\phi = 2 \tan^{-1} \frac{1}{2} \tau \ ,$$

where $\tau_1 = 0$.

Here τ_1 is a parameter defining the trailing edge thickness of the control (Fig.3b),

$$\tau_1 = \frac{t_1}{c} \ ,$$

where t_1 is the control thickness at the trailing edge.

In a few cases with raked tip controls on delta wings (see Nos. 3 and 4 in Table 1), the control profile was a continuation of the wing profile (NACA 0005-63), so that inevitably the thickness-chord ratio of the control varied across its span. Initially, τ was defined at an arbitrary spanwise station. This value was later checked by determining a mean value of τ across the span.

$$\tau_{mean} = \int_0^1 \left(\frac{t_{max}}{c}\right) d\left(\frac{y}{b}\right) ,$$

where t_{max} is the maximum thickness of the control at a spanwise distance y measured from the root. The agreement between the two values was found to be good. In these cases ϕ was again defined as

$$\phi = 2 \tan^{-1} \left(\frac{\tau}{2}\right) .$$

In the analysis of the effect of hinge line location some of the data used was for controls of double-wedge cross section. In all cases, the rear wedge of the control was a continuation of the wing section (Fig. 3c), and ϕ was taken to be the included angle at the trailing edge.

The hinge moment coefficient C_H was defined as

$$C_H = \frac{H}{qS\bar{\bar{c}}} ,$$

where H is the hinge moment measured about the hinge line (positive when it tends to deflect the trailing edge downwards), q is the free stream kinetic pressure and $\bar{\bar{c}}$ is the control aerodynamic mean chord.

i.e.
$$\bar{\bar{c}} = \int_0^b c^2 dy \Bigg/ \int_0^b c dy = \frac{1}{S}\int_0^b c^2 dy .$$

Hinge moment data of NASA origin for controls both with and without leading edge sweepback usually has 2M' as the reference volume, where M' is defined as the first moment of area of the control behind the hinge line about the hinge line. In all cases the data has been corrected to the standard form of this analysis, viz.

$$C_H = \frac{H}{qS\bar{\bar{c}}} .$$

For tapered controls with swept leading edges, with the hinge line a line of constant percentage chord (Figs. 1b and 1d), we have

$$S\bar{\bar{c}} = \int_0^b c^2 dy = bc_r^2\left[\lambda + \frac{(1-\lambda)^2}{3}\right] ,$$

and

$$2M' = \left(1 - \frac{h}{c}\right)^2 bc_r^2\left[\lambda + \frac{(1-\lambda)^2}{3}\right]\cos\Lambda_{H.L.} ,$$

i.e.

$$2M' = S\bar{\bar{c}}\left(1 - \frac{h}{c}\right)^2 \cos\Lambda_{H.L.} ,$$

where c_r is the control root chord, λ is the control taper ratio, and h/c and $\Lambda_{H.L.}$ are the chordwise location and sweepback angle of the hinge line respectively. For tapered controls with unswept leading edges (Figs. 1a and 1c), and with the hinge line at the leading edge, it follows that,

$$2M' \equiv S\bar{\bar{c}} .$$

For rectangular controls with raked tips (Fig. 1e),

$$S\bar{\bar{c}} = c^3\left[\frac{b}{c} - \frac{2}{3}\cot\Lambda_T\right] ,$$

and

$$2M' = \left(1 - \frac{h}{c}\right)^2\left[\frac{b}{c} - \frac{1}{3}\left(1 - \frac{h}{c}\right)\cot\Lambda_T\right]$$

where c is the constant chord of the inboard part of the control and Λ_T is the sweepback angle of the tip. In the above expression for $S\bar{\bar{c}}$ and 2M' for both tapered controls and rectangular controls with raked tips, b should be replaced by b/2 when the control is mounted on a reflection plane or body.

The control deflection (η) was always measured normal to the hinge line, and was defined as being positive when the trailing edge was deflected downwards. In general, the variation of C_H with η was non linear, and the present analysis has been restricted to the initial hinge moment curve slope, $dC_H/d\eta$ at zero η.

Full details of the analysis are given in Table 2.

4 $dC_H/d\eta$ AT SUPERSONIC SPEEDS

4.1 Linear theory for rectangular controls

Two dimensional

For a rectangular control of infinite aspect ratio, the expressions for lift coefficient C_L and aerodynamic centre position x_a, are:-

$$\frac{dC_L}{d\eta} = \frac{4}{\beta} \quad \text{and} \quad \frac{x_a}{c} = \frac{1}{2} \quad , \tag{1}$$

where $\beta = \sqrt{M^2-1}$.

If h/c is the chordwise location of the hinge line,

then
$$-\frac{dC_H}{d\eta} = \frac{2}{\beta} - \frac{4}{\beta} \cdot \frac{h}{c} \quad . \tag{2}$$

For h/c = 0, this becomes

$$-\frac{dC_H}{d\eta} = \frac{2}{\beta} \quad . \tag{3}$$

Rectangular control with two "free" tips

This solution is identical to that of an isolated rectangular wing[4]. From

and
$$\left.\begin{aligned} \frac{dC_L}{d\eta} &= \frac{4}{\beta}\left(1 - \frac{1}{2A\beta}\right) \quad , \\ \frac{x_a}{c} &= \frac{1}{2}\left[1 - \frac{1}{3(2A\beta-1)}\right] \quad , \end{aligned}\right\} \tag{4}$$

we have for $h/c \neq 0$,

$$-\frac{dC_H}{d\eta} = \frac{4}{\beta}\left(1 - \frac{1}{2A\beta}\right)\left\{\frac{1}{2}\left[1 - \frac{1}{3(2A\beta-1)}\right] - \frac{h}{c}\right\} \quad , \tag{5}$$

which is valid for $\beta A > 1$ (Fig.4a).

Equation (5) can be written as,

$$-\frac{dC_H}{d\eta} = \frac{2(2A\beta-1)}{A\beta^2}\left[\frac{(3A\beta-2)}{3(2A\beta-1)} - \frac{h}{c}\right] \quad , \tag{6}$$

which for $h/c = 0$ becomes

$$-\frac{dC_H}{d\eta} = \frac{2}{\beta} - \frac{4}{3}\frac{1}{A\beta^2} \quad . \tag{7}$$

For $1/2 < \beta A < 1$, the expressions for $dC_L/d\eta$ and x_a/c given in Ref.4 are considerably more complex, and are not reproduced here. For most controls of practical size and thickness, linear theory is not likely to be accurate over this range of βA, since the flow will be transonic in nature.

Rectangular control with two 'bounded' tips

The expression for $dC_H/d\eta$ has been obtained by Tucker and Nelson[5] for a control on a rectangular planform wing, and for $h/c = 0$ it is

$$-\frac{dC_H}{d\eta} = \frac{2}{\beta} - \frac{8}{3\pi} \times \frac{1}{A\beta^2} \quad . \tag{8}$$

The range of validity of this expression depends upon control and wing planforms. The limit due to control planform is identical to that for a control with 'free' tips, viz.

$$\beta A \geqslant 1 \quad . \qquad \text{(Fig.4a)}$$

The two limits due to wing planform are

$$\beta A \geqslant \frac{b}{b_w - 2y_c - 2b} \quad , \qquad \text{(Fig.4b)}$$

and

$$\beta A \geqslant \frac{b}{2y_c} \quad , \qquad \text{(Fig.4c)}$$

where b_w is the wing span and y_c is the distance from a reflection plane to the inboard edge of the control. In the case of a control situated next to a reflection plane, only the first of these two limits applies. Putting $y_c = 0$ in the expression and writing $b/2$ for b and $A/2$ for A we obtain

$$\beta A \geqslant \frac{b}{b_w - b} \quad . \qquad \text{(Fig.4d)}$$

The above expression for $dC_H/d\eta$ applies to controls with 'bounded' tips on any wing; in each case, however, the first of the two limits due to wing planform shape is different. In the case of a delta wing or any wing with a raked tip, this limit is

$$\beta A \geq \frac{(1 + \beta \cot \Lambda_{L.E.})\, b}{(b_w - 2y_c - 2b)} \quad . \qquad \text{(Fig. 4e)}$$

For $\beta A \leq 1$, the expression for $dC_H/d\eta$ can be obtained from Ref. 5.

Rectangular control with one 'free' tip and one 'bounded' tip

From reference 5 we have for $h/c = 0$

$$-\frac{dC_H}{d\eta} = \frac{2}{\beta} - \frac{2}{3}\left(\frac{2+\pi}{\pi}\right)\frac{1}{A\beta^2} \quad , \qquad (9)$$

where the limits are

$$\beta A \geq 1 \quad , \qquad \text{(Fig. 4a)}$$

and

$$\beta A \geq \frac{b}{b_w - 2b} \quad . \qquad \text{(Fig. 4f)}$$

For

$$\beta A \leq \frac{b}{b_w - 2b} \quad ,$$

and

$$\beta A \geq 1 \quad ,$$

the expression for $dC_H/d\eta$ is given in Ref. 5.

4.2 Comparison of theoretical and experimental hinge moments coefficients

4.2.1 Controls with hinge line at leading edge

Available experimental data for controls with the hinge line at the leading edge is shown in Fig. 5. The data have been plotted in the form of the usual supersonic similarity parameters ($-1/A\ dC_H/d\eta$ against $A\sqrt{M^2-1}$). Linear theory estimates for a two dimensional control, a rectangular control with 'free' tips, and a rectangular control with 'bounded' tips, are also shown in this figure. The experimental data collapse fairly well onto a single curve for $2 < A\sqrt{M^2-1} < 20$, the widest scatter (80% of the data within ±10% of the mean curve) occurring at low values of $A\sqrt{M^2-1}$. No significant differences are present between the data for different types of planform, and although at small values of $A\sqrt{M^2-1}$, the results for controls having 'bounded' tips fall slightly below those for controls having 'free' tips (the opposite effect to that predicted by theory), the differences are not marked. At all values of $\Lambda\sqrt{M^2-1}$ the experimental points are some 20% less than the theoretical estimates.

There are several possible reasons for the discrepancy between experiment and linear theory: the finite thickness of the controls, interference effects from bodies, and the effect of gaps between control and reflection plane or body.

Tucker and Nelson[5] have estimated the characteristics of rectangular trailing edge controls having finite thickness with plane upper and lower surfaces. Their method was to assume that the use of third order approximations to the pressure coefficients, altered only the magnitude of the pressures on the control, the shape of the pressure distribution remaining unaltered; i.e. if the ratio of the third order approximation to the linear approximation for $dC_H/d\eta$ of a two dimensional control with thickness is calculated, this factor can then be applied to the linear theory estimate for a rectangular control. For small control deflection the thickness factor depends only on the trailing edge included angle ϕ, and is given by,

$$K_\phi = 1 - \frac{C_2}{C_1}\phi + \frac{3}{4}\frac{C_3}{C_1}\phi^2 \quad , \tag{10}$$

where C_1, C_2 and C_3 are constants in the Busemann third order approximation for the pressure coefficient in two dimensional, isentropic, supersonic flow, viz.

$$C_p = C_1\theta + C_2\theta^2 + C_3\theta^3 \quad , \tag{11}$$

where θ is the flow deflection angle, positive for a compression and negative for an expansion, and

$$\left.\begin{aligned} C_1 &= \frac{2}{(M^2-1)^{\frac{1}{2}}} \quad , \\ C_2 &= \frac{(\gamma+1)\,M^4 - 4(M^2-1)}{2(M^2-1)^2} \quad , \\ C_3 &= \frac{1}{6(M^2-1)^{7/2}}\left[(\gamma+1)\,M^8 + (2\gamma^2-7\gamma-5)\,M^6 + 10(\gamma+1)\,M^4 - 12M^2 + 8\right] . \end{aligned}\right\} \tag{12}$$

Values of C_1, C_2 and C_3 are tabulated in several sources, e.g. Ref.5 and 6. Shock expansion theory has been used[7] to obtain a thickness factor for linear theory, however, it is cumbersome, as the factor is dependent upon the wing profile ahead of the control, and it requires a separate calculation for each deflection angle. Similarly, the use of the Busemann third order approximation with the additional constant D included in the case of oblique shock compressions[6], viz.

$$C_p = C_1\theta + C_2\theta^2 + (C_3-D)\,\theta^3 \quad , \qquad (13)$$

where

$$D = \frac{\frac{(\gamma+1)\,M^4}{12}\left[\left(\frac{5-3\gamma}{4}\right)M^4 + (\gamma-3)\,M^2 + 2\right]}{(M^2-1)^{7/2}} \quad , \qquad (14)$$

is complicated in that the wing shape ahead of the control has to be included in the calculation. Moreover, the magnitude of D is quite small, say 10% of C_3, so that only a small gain in accuracy results from its inclusion. K_ϕ, calculated from equation number 10, is plotted in Fig.6 for positive values of ϕ $(\tau_1 < \tau)$ at several Mach numbers. It is always less than unity for positive ϕ, and in general it decreases with increasing Mach number. The limit of applicability was obtained in Reference 5 by comparing the third order approximation with an exact calculation using shock-expansion theory on a double wedge aerofoil. A discrepancy of 10% between the two values of K_ϕ was regarded as the limit to which third order theory could accurately be applied.

Where a trailing edge control is situated next to a circular cross section body, in theory a further reduction of $dC_H/d\eta$ occurs, because the body does not act as a perfect reflection plane. The principles of wing body interference are explained in some detail by Pitts, Nielsen, and Kaattari in Reference 8, and it is from this source that the relevant factor, $k_{W(B)}$, is reproduced in Fig.7. In the present context, $k_{W(B)}$ is defined as the ratio of the lift on a control in the presence of a circular section body to the lift on an isolated control (of aspect ratio twice that of the exposed panel, c.f. Section 3). The body is considered to be at zero incidence, and the lift is produced by deflection of the control. Fig.8 shows the interference effects on aerodynamic centre (again obtained from Ref.8). A factor K_x is defined as

$$K_x = \frac{\left(\frac{x_a}{c}\right)_{control + body} - \frac{h}{c}}{\left(\frac{x_a}{c}\right)_{control} - \frac{h}{c}} , \qquad (15)$$

where x_a is the chordwise location of the aerodynamic centre. Fig.9 shows values of K_x calculated for controls with the hinge line at the leading edge. In Ref.8 it was recommended that the linear theory estimates for $k_{W(B)}$ and x_a/c should be used for $A\sqrt{M^2-1} > 2$, and the slender body value for $A\sqrt{M^2-1} < 2$.

No attempt has been made in this analysis to correct the hinge moment coefficients for the effect of gaps between controls and bodies or reflection planes, due principally to the limited amount of information on gaps available in the present data. However, slender body theory[9] does indicate that the component lift on wing body combinations is significantly reduced by the presence of gaps. Measurements have been made by Dugan[10] of the component lift on a 60° delta wing-body combination at M = 1.4 for various gap widths. His results, in the form of a gap factor K_g (ratio of lift on wing with gap present to lift on wing with no gap), are shown in Fig.10, together with a theoretical curve again taken from Ref.10 but originally derived using the theory of Ref.9. The experimental results, although for a wing-body combination having a body radius to semi-span ratio (r/s_W) of 0.216, should be applicable to a control-body combination having the same value of r/s. The measured values of K_g are compared with theory only for values of g/s_W greater than 0.03. Here, the measured values exceed theory by about 10% for values of gap to semi-span ratio (g/s_W) above 0.03, probably due to viscous effects in the gap. Obviously for large gaps ($g/s > 0.004$ say), the effect on control lift and hinge moment is likely to be important, but for most practical sizes of gap to semi-span ratio ($g/s < 0.004$), it is unlikely that the effects will be too significant. This is confirmed by the experimental correlation in Fig.11. Here the basic data have been factored to allow for both control thickness and body interference, viz.

$$\left[\frac{dC_H}{d\eta}\right]'' = \frac{1}{K_\phi} \times \frac{1}{K_x} \times \frac{1}{k_{W(B)}} \times \frac{dC_H}{d\eta} . \qquad (16)$$

The introduction of these factors gives a much better correlation than that shown in Fig.5. Although the differences between the theoretical solutions for a control with 'free' and 'bounded' tips are not very large, the 'free' tip solution seems to indicate better the trend of the experimental results at low values of $A\sqrt{M^2-1}$.

4.2.2 Effect of hinge line location

Fig. 12 shows hinge moment derivatives measured on controls with various hinge line locations. The values of $dC_H/d\eta$ have been corrected for control thickness and body radius in the manner described in Section 4.2.1, and are plotted as $1/A\,[dC_H/d\eta]''$ against $A\sqrt{M^2-1}$. The trend of the results with hinge line location is sensible, but in order to make an accurate comparison with theory the data has been replotted in Fig. 13 against hinge line location for various values of $A\sqrt{M^2-1}$. The agreement between experiment and theory is shown in Fig. 13 to be reasonably good.

4.2.3 Effect of trailing edge thickness

An increase in the trailing edge thickness of the control gives a corresponding increase in $dC_H/d\eta$ (Fig. 14a). However, if the values of $dC_H/d\eta$ are corrected for trailing edge angle ϕ and body interference effects using the method described in Section 4.2.1, then the data for all trailing edge thicknesses collapse onto the linear theory estimate for a rectangular control with free tips (Fig. 14b). This result means that $dC_H/d\eta$ for a control whose upper and lower surfaces are parallel $(\tau_1 = \tau)$, is identical to that on a control with zero thickness. For negative values of $\phi(\tau_1 > \tau)$, K_ϕ is always greater than unity which indicates that $(dC_H/d\eta)$ continues to increase as τ_1 is increased above τ. Although Fig. 6 gives values of K_ϕ for positive ϕ only, values of K_ϕ for negative ϕ can easily be obtained from the expression given in Section 4.2.1.

5 $dC_H/d\eta$ AT TRANSONIC SPEEDS

5.1 Theoretical considerations

Similarity parameters for use at transonic speeds have been developed by several authors, e.g. Von Karman[11], Spreiter[12,13], Busemann[14] and Harder[15]. McDevitt[16] showed that the parameters for the initial lift curve slope of uncambered wings of finite aspect ratio, as originally put forward by Spreiter[12], can be written in the following manner:

$$(\gamma+1)\left(\frac{t}{c}\right)_w^{1/3}\left(\frac{dC_L}{d\alpha}\right)_{\alpha=0} = f\left\{\frac{M^2-1}{\left(\frac{t}{c}\right)_w^{2/3}(\gamma+1)^{2/3}},\ A_w\left(\frac{t}{c}\right)_w^{1/3}(\gamma+1)^{1/3}\right\}. \quad (17)$$

Similarly it can be shown that,

$$(\gamma+1)\left(\frac{t}{c}\right)_W^{1/3}\left(\frac{dC_m}{d\alpha}\right)_{\alpha=0} = g\left\{\frac{M^2-1}{\left(\frac{t}{c}\right)_W^{2/3}(\gamma+1)^{2/3}}\ ,\ A_W\left(\frac{t}{c}\right)_W^{1/3}(\gamma+1)^{1/3}\right\}\ , \quad (18)$$

where f and g are some unspecified functions of the parameters in the brackets, γ is the ratio of specific heats (if only one fluid medium is being considered, functions of γ can be left out of the equation), $(t/c)_W$ and A_W are the thickness chord ratio and aspect ratio of the wing respectively.

The analysis of Busemann[14] and Harder[15] produced an alternative form for the similarity parameters,

$$(\gamma+1)^{1/3} M^{2/3}\left(\frac{t}{c}\right)_W^{1/3}\left(\frac{dC_L}{d\alpha}\right)_{\alpha=0} = f\left\{\frac{M^2-1}{M^{4/3}(\gamma+1)^{2/3}\left(\frac{t}{c}\right)_W^{2/3}}\ ,\right.$$

$$\left. A_W\left(\frac{t}{c}\right)_W^{1/3}(\gamma+1)^{1/3} M^{2/3}\right\}\ , \quad (19)$$

and similarly for $dC_m/d\alpha$. Spreiter[13] has shown that this second form of the similarity parameters improved the correlation between experiment and transonic flow theory in certain cases, e.g. the drag of a two dimensional single wedge section. However, McDevitt[16], using the simpler parameters put forward by Spreiter originally, obtained a good correlation of the experimental characteristics of a family of rectangular wings. In view of this result, and because of the increased complexity of the modified parameters, it was decided to use the simpler parameters in an attempt to correlate hinge moments at transonic speeds.

Although at subsonic speeds control hinge moments depend on the wing shape and the relative proportions of control and wing, the development of regions of supersonic flow over the wing surface at high subsonic Mach numbers would probably decrease the influence of the wing on $dC_H/d\eta$. At $M = 1.0$ $dC_H/d\eta$ should be independent of the wing planform. There is some reason, therefore, to expect a correlation of $dC_H/d\eta$ both at high subsonic speeds as well as sonic and low supersonic speeds based solely on control parameters.

In Appendix A, using shock-expansion theory, an approximate expression is developed for $dC_H/d\eta$ of a rectangular control on an infinite double wedge wing at Mach numbers of 1.0 and above. The numerical values obtained are reproduced below.

$A\tau^{1/3}$	$-\tau^{1/3}\frac{dC_H}{d\eta}$			
	$\frac{M^2-1}{\tau^{2/3}} = 0$	0.5	1.0	2.0
0.444	0.186	0.179	0.173	0.165
0.887	0.726	0.699	0.672	0.643
1.774	1.012	0.974	0.937	0.896
3.549	1.161	1.117	1.074	1.027
5.323	1.208	1.162	1.118	1.069
∞	1.304	1.255	1.207	1.154

5.2 Correlation of experimental data

5.2.1 Controls with hinge line at leading edge

Fig.15 shows a plot of $-\tau^{1/3}\,[dC_H/d\eta]'$ against $M^2-1/\tau^{2/3}$ for controls with the hinge line at the leading edge. $[dC_H/d\eta]'$ is the hinge moment derivative corrected for body interference effects on lift only (slender body theory) in the manner described in 4.2.1, i.e.

$$\left[\frac{dC_H}{d\eta}\right]' = \frac{1}{k_{w(B)}} \times \frac{dC_H}{d\eta} ,$$

where $k_{w(B)}$ is the slender body value (Fig.7). Because $\tau^{1/3}\,[dC_H/d\eta]'$ is also a function of the other transonic similarity parameter $A\tau^{1/3}$, the only deduction possible from Fig.15 is that there is a marked increase in $-dC_H/d\eta$ between subsonic and supersonic speeds. Using the data in Fig.15, $\tau^{1/3}\,[dC_H/d\eta]'$ has been replotted against $A\tau^{1/3}$ for various values of $M^2-1/\tau^{2/3}$ (Fig.16).

The correlation of the experimental $dC_H/d\eta$ is only fair at subsonic speeds (Fig.16a,b,c), and there is appreciable scatter. In general for $M^2-1/\tau^{2/3} = -2$ and -1, the experimental data approaches the linear theory[17] estimate for $dC_m/d\alpha$ about the leading edge of an isolated wing at small values of $A\tau^{1/3}$. For large values of $A\tau^{1/3}$, the experimental values are at about 50% of the linear theory value. It is possible that the correlation at subsonic speeds is fortuitous, since the range of wing planforms in the data is rather restricted (mainly 60° deltas), and the ratios of control chord to wing root chord are all about the same value (0.1).

At supersonic speeds the correlation is fairly good (Fig. 16d,e,f,g). At $M = 1.0$ the experimental hinge moments are in good agreement with the experimental values of $dC_m/d\alpha$ measured by McDevitt[16] on isolated rectangular wings for $A\tau^{1/3} \leq 2$. At $M^2-1/\tau^{2/3} = 0.5$ and 1.0 the pitching moment data falls slightly below the hinge moment data. The theory of Appendix A agrees well with experiment at $M^2-1/\tau^{2/3} = 2.0$, but tends to overestimate at lower values of $M^2-1/\tau^{2/3}$. This theory gives the aerodynamic centre position of the two dimensional control at 50% c for all positive values of $M^2-1/\tau^{2/3}$. However, it is shown in Section 5.2.2 that in practice[18] the aerodynamic centre position of a control with $A\tau^{1/3} = 5.1$ is located up to 0.085 c forward of this point, for $M \geq 1.0$. The results of Ref. 16 showed that for an isolated rectangular wing, the aerodynamic centre position was identical to the two dimensional value for $A\tau^{1/3} > 1$ at supersonic speeds and $A\tau^{1/3} > 2.5$ at subsonic speeds. If it can be assumed that a similar result holds for rectangular controls, then the aerodynamic centre position of the control with $A_c\tau^{1/3} = 5.1$ can be used to obtain a factor (ratio of (x_a/c) experiment to (x_a/c) theory) which can then be applied to the theory.

$\frac{M^2-1}{\tau^{2/3}}$	$\left(\frac{x_a}{c}\right)_{experiment}$ $A\tau^{1/3} = 5.096$	$\left(\frac{x_a}{c}\right)_{theory}$ $A\tau^{1/3} = \infty$	Factor
0	0.415	0.500	0.830
0.5	0.443	0.500	0.886
1.0	0.460	0.500	0.920
2.0	0.475	0.500	0.950

The modified theory (valid for $A\tau^{1/3} > 1$) is in much better agreement with experiment especially at $M = 1.0$ (Fig. 16d,e,f,g).

An attempt was made to allow for the effects of the boundary layer thickness on the control thickness-chord ratio. The effective value of τ was assumed to be

$$\tau \text{ effective} = \tau + \frac{2(\delta^*_{turb})_{mean}}{c} , \qquad (20)$$

where $(\delta^*_{turb})_{mean}$ is the mean value across the control span of the displacement thickness of a flat plate boundary layer, with transition at the wing leading edge. The use of this modified value of τ did not result in any improvement in the correlation of the experiment data.

The discussion in Section 4.2.1 on gap effects at supersonic speeds will apply equally here, but as in that case no further analysis is possible because of the lack of information on gaps in the present data.

5.2.2 Effect of hinge line location

Because $dC_H/d\eta$ is dependent upon such a large number of parameters at transonic speeds, it was not possible to determine the variation of $\tau^{1/3} [dC_H/d\eta]'$ with h/c by plotting data for different controls on the same figure. However, Fig.17 shows the effect on $\tau^{1/3} [dC_H/d\eta]'$ of varying the hinge line location (from h/c = 0.065 to 0.507) for one particular control[18] of $A\tau^{1/3} = 5.096$. For $M < 1.0$ $dC_H/d\eta$ varies linearly with h/c for h/c < 0.50, whereas for $M > 1.0$ the range of linearity is restricted to h/c < 0.30. The location of the control aerodynamic centre position as obtained from the linear portion of the curve in Fig.17 is shown in Fig.18, together with the experimental values[19] for a control of $A\tau^{1/3} = 4.201$, the linear theory[4,17] estimate for an isolated rectangular wing with $A\tau^{1/3} = 5.096$, and the experimental values for an isolated rectangular wing[16]. The agreement between the measured values for the two controls is good, the discrepancy at positive values of $M^2-1/\tau^{2/3}$ is probably due to a non linearity in the curves of $\tau^{1/3} [dC_H/d\eta]'$ against h/c for the control[19] with $A\tau^{1/3} = 4.201$, similar to that observed in Fig.17. (Only two hinge line locations were tested on this control, h/c = 0.07 and 0.50.)

5.2.3 Effect of trailing edge thickness

In general an increase of $-dC_H/d\eta$ results from increasing the trailing edge thickness of the control (Fig.19). The factor $K\tau_1$ is defined as the ratio of $(dC_H/d\eta)_{\tau_1 \neq 0}$ to $(dC_H/d\eta)_{\tau_1 = 0}$, and is shown in Figs.20 and 21. Although at subsonic speeds the variation of K_{τ_1} with $M^2-1/\tau^{2/3}$ for the two configurations appears inconsistent (Fig.20), values of K_{τ_1} do show good agreement at $M = 1.0$ with the two dimensional shock-expansion theory of Appendix A (Fig.21).

6 CONCLUSIONS

Similarity rules have been used at supersonic and transonic speeds to obtain a correlation of experimental values of $dC_H/d\eta$ and to compare these values with theory.

At supersonic speeds for controls with the hinge line at the leading edge, $dC_H/d\eta$ can be predicted with reasonable accuracy (80% of data within ±10%) within the range, $2 < A\sqrt{M^2-1} < 20$, using the supersonic linear theory solution for a control with 'free' tips, and applying corrections to allow for the effects of body interference and control thickness, i.e.

$$-\frac{dC_H}{d\eta} = K_\phi \times K_x \times k_{w(B)} \times \left\{\frac{2}{\beta} - \frac{4}{3A\beta^2}\right\} , \tag{21}$$

(see Figs. 6, 7, 9 and 11).

For controls with the hinge line not at the leading edge the accuracy is about the same (±10% of value for $h/c = 0$) within the range, $6 < A\sqrt{M^2-1} < 14$. In this case,

$$-\frac{dC_H}{d\eta} = K_\phi \times K_x \times k_{w(B)} \times \left\{\frac{2(2A\beta-1)}{A\beta^2}\right\}\left\{\frac{(3A\beta-2)}{3(2A\beta-1)} - \frac{h}{c}\right\} , \tag{22}$$

(see Figs. 6, 7, 8, 9 and 13).

At transonic speeds for controls with the hinge line at the leading edge and with $\tau < 0.13$, $dC_H/d\eta$ can be predicted, again with reasonable accuracy (±10%), above $M = 1$ $(0 < M^2-1/\tau^{2/3} < 2)$, using shock expansion theory with an empirical correction factor applied to the aerodynamic centre position and a slender body factor to allow for body interference on lift (see Figs. 7 and 16 and Appendix A). Below $M = 1$ the experimental correlation is only fair (a scatter of ±20% on the mean value), and even this may be fortuitous since the range of wing planform in the data is restricted to 60° delta, and the ratios of control chord to wing root chord are all very similar (around 0.1).

The effect of trailing edge thickness on $dC_H/d\eta$ can be estimated at supersonic speeds by merely adjusting the factor K_ϕ, and at $M = 1$ there is some evidence that it can be predicted using the two dimensional shock-expansion theory of Appendix A.

Appendix A

$dC_H/d\eta$ FOR A RECTANGULAR CONTROL ON AN INFINITE WING OF DOUBLE WEDGE CROSS SECTION AT TRANSONIC MACH NUMBERS

The theoretical solution for the inviscid transonic flow past a double wedge profile has been known for some time[20,21]. For free stream Mach numbers between unity and the value appropriate to bow shock attachment, theory predicts subsonic flow over the forward facing wedge with the local Mach number increasing from zero at the leading edge to a value of unity at the shoulder (Figs.22 and 23). The flow then undergoes a supersonic expansion around the shoulder. For a given value of $(t/c)_w$ the local Mach number immediately behind the shoulder, identical to the value given by a Prandtl-Meyer expansion, is independent of free stream Mach number. Because some of the expansion waves from the shoulder are reflected from the sonic line as compression waves, the local Mach number decrease slightly between the shoulder and the trailing edge. At the trailing edge the flow then returns to the free stream direction by means of an oblique shock compression.

Since both the free stream and the local flow over the rear half of the aerofoil are supersonic, it is possible to distort or deflect part of the profile near the trailing edge without affecting the flow over the rest of the profile, providing that no detached shock waves are produced by these local changes of slope.

In order to calculate the hinge moment on a control some simplifying assumptions have been made. For the majority of the calculations the above mentioned variation of local Mach number over the rear wedge has been ignored. The Mach number was taken to be constant at the Prandtl-Meyer expansion value (Fig.23).

With the flow model shown in Figs.22 and 23, and with η arbitrarily taken to be 1°, the hinge moment derivative, $dC_H/d\eta$, of a two dimensional control was calculated using shock-expansion theory. The results at $M = 1.0$ are summarized in the following table:-

$$\frac{M^2 - 1}{\tau^{2/3}} = 0$$

ϕ°	τ	$-\frac{dC_H}{d\eta}$	$-\tau^{1/3}\frac{dC_H}{d\eta}$
5	0.0873	2.939	1.304
10	0.1750	2.280	1.275
15	0.2633	1.931	1.238

The use of the transonic similarity parameter, $\tau^{1/3}\, dC_H/d\eta$,[16] was found to give an adequate although not perfect collapse of the theoretical estimates for different values of τ. All further calculations have been performed with $\phi = 5^\circ$.

Under the assumptions of the theory, the Mach number over the rear wedge of the aerofoil is independent of free stream Mach number, and dependent only on ϕ. It follows that the nondimensional parameter,

$$\frac{\text{pressure difference between control upper and lower surfaces,}}{\text{local total pressure}}$$

is also independent of free stream Mach number. If we assume that the loss of total pressure through shock waves can be ignored, (for $\phi = 5^\circ$ and $M^2-1/\tau^{2/3} = 2.0$, then $M = 1.181$, and the loss in total pressure through the bow shock wave amounts to $\frac{1}{2}\%$), then the variation of $dC_H/d\eta$ with free stream Mach number arises through the variation of the ratio of total pressure to kinetic pressure with Mach number. Calculated values, in transonic similarity form, are shown below.

$\phi = 5^\circ$

$\frac{M^2-1}{\tau^{2/3}}$	$-\frac{dC_H}{d\eta}$	$-\tau^{1/3}\frac{dC_H}{d\eta}$
0	2.939	1.304
0.5	2.830	1.255
1.0	2.722	1.207
2.0	2.601	1.154

The effect of trailing edge thickness for a control with a linear thickness distribution, is independent of Mach number and is shown in the following table:-

$\tau = 0.0873$

$\frac{\tau_1}{\tau}$	K_{τ_1}
0	1.000
0.5	1.124
1.0	1.325
1.5	1.726

The effect of finite aspect ratio has been obtained by multiplying the two dimensional values calculated from transonic theory by the ratio of the supersonic linear theories for finite and infinite aspect ratio. The supersonic linear theories were based on the wing local Mach number just ahead of the control, and the finite aspect ratio value was calculated for a control with 'free' tips, since this gave the best agreement between theory and experiment at supersonic speeds. The effect of finite aspect ratio is shown in the following table:

$\phi = 5^\circ \quad \tau = 0.0873 \quad \tau_1/\tau = 0$

A	$A\tau^{1/3}$	$-\tau^{1/3}\dfrac{dC_H}{d\eta}$			
		$\dfrac{M^2-1}{\tau^{2/3}} = 0$	0.5	1.0	2.0
1.0	0.444	0.186	0.179	0.173	0.165
2.0	0.887	0.726	0.699	0.672	0.643
4.0	1.774	1.012	0.974	0.937	0.896
8.0	3.549	1.161	1.117	1.074	1.027
12.0	5.323	1.208	1.162	1.118	1.069
∞	∞	1.304	1.255	1.207	1.154

The above values are strictly valid, only within the range

$$0 < \frac{M^2-1}{(\gamma+1)^{2/3}\left(\frac{t}{c}\right)_w^{2/3}} < 1.26 \quad .$$

The upper limit* is the value predicted by transonic small perturbation theory[21] for an attached shock wave at the leading edge of the wing with uniform sonic flow behind it over the front wedge. If, instead of the wing thickness chord ratio $(t/c)_w$, we use the control thickness parameter τ in the similarity parameter, we arrive at the following limits of validity

$$0 < \frac{M^2-1}{(\gamma+1)^{2/3}\,\tau^{2/3}} < \frac{1.26}{2^{2/3}} = 0.794 \quad ,$$

or

$$0 < \frac{M^2-1}{\tau^{2/3}} < 1.423 \quad .$$

However, an exact calculation performed using shock expansion theory over the entire wing ($\phi = 5^\circ$) at $M^2-1/\tau^{2/3} = 2.0, (M^2-1/(\gamma+1)^{2/3}\,\tau^{2/3} = 1.424)$,

*The exact value of the transonic similarity parameter, $M^2-1/(\gamma+1)^{2/3}\,(t/c)_w^{2/3}$, at this condition for a wedge of 5° included angle is 1.451.

again arbitrarily taking the control deflection to be 1°, gave a value of -1.161 for $\tau^{1/3}\ dC_H/d\eta$ compared with -1.154 using the approximate method. It is clear, therefore, that the approximate theory compares favourably with exact theory at values of $M^2-1/\tau^{2/3}$ well above the limit for bow shock attachment. The assumption of constant Mach number over the rear wedge of the wing means that the estimated two dimensional values of $dC_H/d\eta$ are too small, due to the mean Mach number over the undeflected control being too high. The error is worst for a control of vanishingly small chord at $M = 1.0$, where the correct value of $\tau^{1/3}\ dC_H/d\eta$ is 1.433 compared with the approximate value of 1.304. The correct value was calculated assuming that the Mach number over the rear wedge of the wing is given by $M^2-1/(\gamma+1)(t/c)_w^{2/3} = 1.72$ instead of the Prandtl-Meyer expansion value of 2.07 (see Fig.23). Because the assumed Mach number over the control is too high, the factor applied to the two dimensional $dC_H/d\eta$ for the effect of aspect ratio is also in error, in the opposite sense to the error in the two dimensional $dC_H/d\eta$. For most practical sizes of control the two errors either wholly or partially offset one another. The values shown in the table below are for a control with vanishingly small chord, for a control with finite chord the errors are slightly less.

$$M^2-1/\tau^{2/3} = 0 \quad \phi = 5^{\circ} \quad c \to 0$$

A	$A\tau^{1/3}$	$-\tau^{1/3}\left(\frac{dC_H}{d\eta}\right)_{approx.}$	$-\tau^{1/3}\left(\frac{dC_H}{d\eta}\right)_{exact}$	% error
1.0	0.444	0.186	0.143	+30.1
2.0	0.887	0.726	0.725	0
4.0	1.774	1.012	1.072	-5.6
8.0	3.549	1.161	1.252	-7.3
∞	∞	1.304	1.433	-9.0

The effect of finite span on the pressure distribution over double wedge cross section wings at transonic speeds above $M = 1.0$, has been investigated experimentally by Vincenti[22]. His results shewed that for wings of finite aspect ratio, the locus of the intersection of the sonic line with the wing surface is a curve, which joins the two wing tip leading edges and is furthest aft at the centre of the wing span. This furthest aft distance of the sonic line is always ahead of the profile shoulder for finite aspect ratios, and moves forward as the aspect ratio decreases. Although this means that there is a large area of supersonic flow over the fore wedge of the wing, the pressure coefficient and hence the local Mach number immediately behind the shoulder, are almost identical to the two dimensional value over the entire wing span. There is, however, an increase of pressure between the shoulder and the trailing edge, consistent in extent with that produced by a Mach line from the shoulder at the tip. A trailing edge control situated in the tip region of a rectangular wing would therefore experience a slightly lower Mach number than one situated inboard of the tip. As in the case of the chordwise Mach number variation, however, the overall effect on $dC_H/d\eta$ may not be too significant.

Table 1 - DETAILS OF WINGS AND CONTROLS

No.	Ref.		$R \times 10^{-6}$	Wing				Control										
				A_w	λ_w	$(\Lambda^o_{L.E.})_w$	Wing section	A	λ	$\Lambda^o_{L.E.}$	b/b_w	$2y_c/b_w$	r/s	h/c	Control section	τ	τ_1/τ	ϕ^o
1a	19	H-n-2 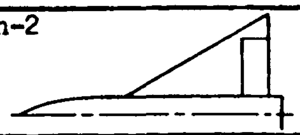	3.1 - 3.9	2.309	0	60.00	Hexagonal $(t/c)_w = 0.040$	8.233	1.0	0	0.616	0	0.198	0.070	Wing profile	0.133	0.141	7.62
1b	19	"	"	"	"	"	"	"	"	"	"	"		0.500	"	"	"	"
2	23	H-n-2 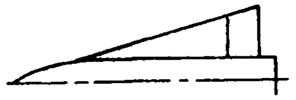	3.4 - 4.7	0.705	0	80.00	Hexagonal $(t/c)_w = 0.030$ to 0.048	4.717	1.0 (raked tip)	0	1.000	0	0.284	0	Wing profile	0.100	0	5.74
3a	24	S-n-2 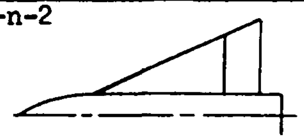	5.6	2.000	0	63.44	NACA 0005-63 streamwise	13.584	1.0 (raked tip)	0	1.000	0	0.180	0	Wing profile	0.104	0	5.96
3b	24	"	"	"	"	"	"	9.257	"	"	"	"		0.332	"	"	"	"
3c	24	"	"	"	"	"	"	"	"	"	"	"		"	Double wedge	-	-	"
3d	24	"	"	"	"	"	"	"	"	"	"	"		"	"	-	-	"
4a	25	S-n-2 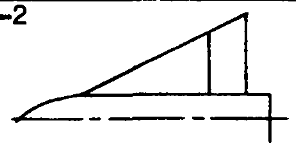	3.7	2.000	0	63.44	NACA 0005-63 streamwise	7.817	1.0 (raked tip)	0	1.000	0	0.180	0	Wing profile	0.104	0	5.96
4b	25	"	"	"	"	"	"	"	"	"	"	"		"	Linear thickness distn.	"	0.500	3.29
5a	26	H-f-2 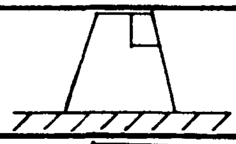	4.9	3.088	0.389	23.00	Hexagonal $(t/c)_w = 0.045$	2.644	0.676	0	0.149	0.702	-	0	Wing profile	0.150	0	8.58
5b	26	H-f-2 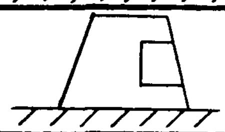	"	"	"	"	"	2.587	0.682	0	0.215	0.272	-	0	"	0.150	0	8.58
5c	26	H-f-2 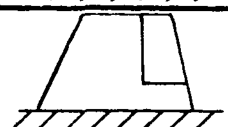	"	"	"	"	"	5.047	0.461	0	0.364	0.272	-	0	"	0.150	0	8.58
5d	26	H-f-2 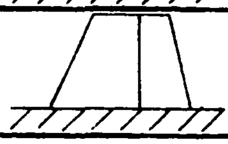	"	"	"	"	"	12.179	0.384	0	1.000	0	-	0	"	0.150	0	8.58
5e	26	"	"	"	"	"	"	"	"	"	"	"	-	"	Linear thickness distn.	"	0.500	4.30
5f	26	"	"	"	"	"	"	"	"	"	"	"	-	"	Constant thickness	"	1.000	0

Table 1 (Contd.) - DETAILS OF WINGS AND CONTROLS

No.	Ref.		$R \times 10^{-6}$	Wing				Control										
				A_w	λ_w	$(\Lambda^{o}_{L.E.})_w$	Wing section	A	λ	$\Lambda^{o}_{L.E.}$	b/b_w	$2y_c/b_w$	r/s	h/c	Control section	τ	τ_1/τ	ϕ^o
6a	27	H-n-2 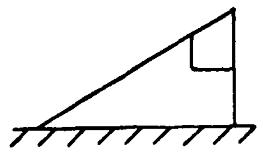	6.3	2.309	0	60.00	Rounded L.E. parallel centre section sharp T.E. $(t/c)_w = 0.030$	2.217	1.0 (raked tip)	0	0.217	0.567	-	0	Wing profile	0.225	0	12.82
6b	27	H-n-2 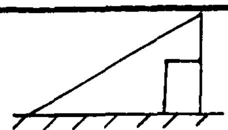	"	"	"	"	"	4.909	1.0	0	0.567	0	-	0	"	0.225	0	12.82
6c	27	H-n-2 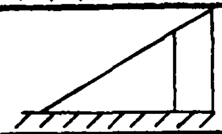	"	"	"	"	"	9.280	1.0 (raked tip)	0	1.0	0	-	0	"	"	"	"
6d	27	"	"	"	"	"	"	"	"	"	"	"	-	"	Linear thickness distn.	"	0.5	6.44
6e	27	"	"	"	"	"	"	"	"	"	"	"	-	"	Constant thickness	"	1.0	0
7a	28	S-n-1 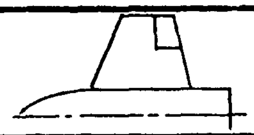	8.6 to 10.4	2.820	0.229	38.65	NACA 65A004 streamwise	4.535	0.304	4.26	0.238	0.524	-	0	Wing profile	0.096	0	5.50
7b	28	"	"	"	"	"	"	"	"	"	"	"	-	"	Constant thickness	"	1.0	0
8a	18	B-n-2 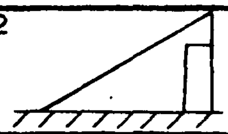	2.2 to 2.7	2.309	0	60.00	Hexagonal $(t/c)_w = 0.040$	10.192	1.0	0	0.661	0	-	0.065	Wing profile	0.125	0	7.16
8b	18	"	"	"	"	"	"	"	"	"	"	"	-	0.242	"	"	"	"
8c	18	"	"	"	"	"	"	"	"	"	"	"	-	0.333	"	"	"	"
8d	18	"	"	"	"	"	"	"	"	"	"	"	-	0.441	"	"	"	"
8c	18	"	"	"	"	"	"	"	"	"	"	"	-	0.507	"	"	"	"
9a	29	S-f-1 	6.1	1.449	0.055	68.00	Sharp L.E. Sharp T.E.	2.047	1.0	0	0.269	0	0.275	0	Wing profile	0.128	0	7.34
9b	30	"	10.5 to 13.5	"	"	"	"	"	"	"	"	"	"	"	"	"	"	"
10a	31	S-f-1 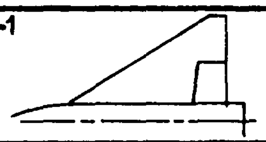	12.5 to 19.4	1.995	0.073	60.00	Round L.E. Sharp T.E. $(t/c)_w = 0.04$	2.978	0.774	9.70	0.481	0	0.266	0	Wing profile	0.087	0	4.97

Table 1 (Contd.) - DETAILS OF WINGS AND CONTROLS

No.	Ref.		$R \times 10^{-6}$	Wing				Control										
				A_w	λ_w	$(\Lambda^o_{L.E.})_w$	Wing section	A	λ	$\Lambda^o_{L.E.}$	b/b_w	$2y_c/b_w$	r/s	h/c	Control section	τ	τ_1/τ	ϕ^o
10b	32	S-f-1	12.5	1.995	0.073	60.00	Round L.E. Sharp T.E. $(t/c)_w = 0.04$	2.978	0.774	9.70	0.481	0	0.266	0	Wing profile	0.087	0	4.97
11	33	H-n-2 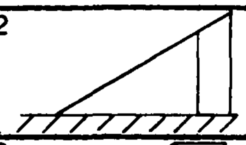	8.0	2.000	0	63.44	Double wedge $(t/c)_w = 0.050$	10.002	1.0 (raked tip)	0	1.0	0	-	0	Wing profile	0.063	0	3.58
12	34	F-n-2 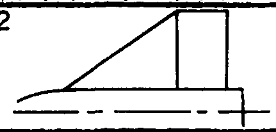	5.8 to 15.0	1.889	0.101	59.92	NACA 65A007 streamwise	10.341	1.0	0	1.0	0	0.246	0.400	Double wedge	-	-	9.20

DETAILS OF CODE IN COLUMN 3 OF TABLE 1

S - sting mounted model
H - half model mounted on reflection plate
B - half model mounted on transonic bump
F - free flight model

n - natural boundary layer transition
f - boundary layer transition artificially fixed at wing leading edge

1 - hinge moment measured on hinge plates cantilevered from wing
2 - hinge moment measured on load cell in body etc. connected to control by circular shaft

Table 2 - DETAILS OF HINGE MOMENT CORRELATION

No.	Ref.	$R \times 10^{-6}$	A	τ	$A\tau^{1/3}$	h/c	M	$-\frac{dC_H}{d\eta}$	$A\sqrt{M^2-1}$	$-\frac{1}{A}\frac{dC_H}{d\eta}$	K_ϕ	$k_{w(B)}$	K_x	$-\frac{1}{A}\left[\frac{dC_H}{d\eta}\right]''$	$\frac{M^2-1}{\tau^{2/3}}$	$-\tau^{1/3}\frac{dC_H}{d\eta}$	$-\tau^{1/3}\left[\frac{dC_H}{d\eta}\right]'$
1a	19	3.1 to 3.9	8.233	0.133	4.201	0.070	0.75	0.684				0.946			-1.630	0.355	0.375
							0.87	0.802				0.946			-0.938	0.416	0.440
							0.98	1.313				0.946			-0.184	0.681	0.720
							1.13	1.511	4.243	0.184		0.946			0.990	0.784	0.829
							1.25	1.416	6.175	0.172	0.862	0.985	0.986	0.206	2.096	0.734	0.776
							1.41	1.181	8.184	0.143	0.848	0.992	0.988	0.172			
							1.62	0.917	10.493	0.111	0.854	0.995	0.993	0.132			
							1.96	0.702	13.878	0.085	0.844	1.000	0.995	0.102			
1b	19	3.1 to 3.9	8.233	0.133	4.201	0.500	0.75	-0.573				0.946			-1.630	-0.297	-0.314
							0.87	-0.716				0.946			-0.938	-0.371	-0.392
							0.93	-0.516				0.946			-0.517	-0.267	-0.282
							0.98	-0.246				0.946			-0.184	-0.128	-0.135
							1.04	0.023				0.946			0.265	0.012	0.013
							1.13	0.057	4.243	0.007		0.946			0.990	0.030	0.032
							1.25	0.178	6.175	0.022	0.862	0.985	0.986	0.026	2.096	0.092	0.097
							1.41	0.235	8.184	0.029	0.848	0.992	0.988	0.034			
							1.62	0.229	10.493	0.028	0.854	0.995	0.993	0.033			
							1.96	0.189	13.878	0.023	0.844	1.000	0.995	0.027			
2	23	3.4 to 4.7	4.717	0.100	2.189	0	0.75	0.759				0.937			-2.030	0.352	0.376
							0.90	1.006				0.937			-0.882	0.467	0.498
							0.95	1.401				0.937			-0.452	0.650	0.694
							1.00	1.612				0.937			0	0.748	0.799
							1.10	1.783				0.937			0.975	0.828	0.883
							1.25	1.806	3.538	0.383	0.864	0.970	0.982	0.465	2.611	0.839	0.865
							1.41	1.559	4.709	0.331	0.879	0.982	0.987	0.388			
							1.62	1.271	6.006	0.269	0.886	0.990	0.990	0.310			
							1.96	0.942	7.967	0.199	0.880	0.995	0.993	0.229			
3a	24	5.6	13.584	0.104	6.389	0	0.60	0.771				0.948			-2.893	0.362	0.382
							0.80	1.054				0.948			-1.628	0.495	0.522
							0.90	1.406				0.948			-0.859	0.661	0.697
							1.20	2.265	9.010	0.166	0.860	1.000	0.990	0.195	1.989	1.065	1.065
							1.30	1.812	11.284	0.133	0.867	1.000	0.992	0.154	3.120	0.852	0.852
							1.50	1.453	15.187	0.107	0.880	1.000	0.994	0.122			
							1.70	1.177	18.675	0.086	0.883	1.000	0.995	0.098			
							1.90	0.983	21.945	0.072	0.880	1.000	0.996	0.082			
3b	24	5.6	9.257			0.332	1.20	0.979	6.140	0.106	0.860	0.980	0.955	0.132			
							1.30	0.805	7.690	0.087	0.867	0.987	0.968	0.104			
							1.50	0.655	10.349	0.071	0.880	0.995	0.981	0.082			
							1.70	0.499	12.727	0.053	0.883	1.000	0.993	0.061			
							1.90	0.462	14.955	0.050	0.880	1.000	0.993	0.058			
3c	24	5.6	9.257			0.332	1.20	0.943	6.140	0.102	0.860	0.980	0.955	0.126			
							1.30	0.757	7.690	0.082	0.867	0.987	0.968	0.099			
							1.50	0.684	10.349	0.074	0.880	0.995	0.981	0.086			
							1.70	0.583	12.727	0.063	0.883	1.000	0.993	0.072			
							1.90	0.438	14.955	0.047	0.880	1.000	0.993	0.054			

Table 2 (Contd.) - DETAILS OF HINGE MOMENT CORRELATION

No.	Ref.	$R \times 10^{-6}$	A	τ	$A\tau^{1/3}$	h/c	M	$-\frac{dC_H}{d\eta}$	$A\sqrt{M^2-1}$	$-\frac{1}{A}\frac{dC_H}{d\eta}$	K_ϕ	$k_{w(B)}$	K_x	$-\frac{1}{A}\left[\frac{dC_H}{d\eta}\right]''$	$\frac{M^2-1}{\tau^{2/3}}$	$-\tau^{1/3}\frac{dC_H}{d\eta}$	$-\tau^{1/3}\left[\frac{dC_H}{d\eta}\right]'$
3d	24	5.6	9.257			0.332	1.20	0.744	6.140	0.080	0.860	0.980	0.955	0.100			
							1.30	0.757	7.690	0.082	0.867	0.987	0.968	0.099			
							1.50	0.583	10.340	0.063	0.880	0.995	0.981	0.073			
							1.70	0.480	12.727	0.052	0.883	1.000	0.993	0.059			
							1.90	0.409	14.955	0.044	0.880	1.000	0.993	0.051			
4a	25	3.7	7.817	0.104	3.676	0	0.60	0.897				0.948			-2.568	0.421	0.444
							0.80	1.312				0.948			-1.445	0.617	0.650
							0.90	1.565				0.948			-0.762	0.736	0.776
							1.30	1.956	6.494	0.250	0.867	0.982	0.984	0.300	2.769	0.920	0.937
							1.53	1.336	9.000	0.171	0.880	0.990	0.990	0.201			
							1.70	1.144	10.747	0.146	0.883	0.996	0.992	0.169			
4b	25	3.7	7.817	0.104	3.676	0	0.60	0.957				0.948			-2.568	0.450	0.474
							0.80	1.402				0.948			-1.445	0.660	0.695
							0.90	1.709				0.948			-0.762	0.803	0.848
							1.30	2.028	6.494	0.259	0.867	0.982	0.984	0.294	2.769	0.954	0.972
							1.53	1.450	9.000	0.186	0.880	0.990	0.990	0.204			
							1.70	1.252	10.747	0.160	0.883	0.996	0.992	0.172			
5a	26	4.9	2.644	0.150		0	1.61	1.242	3.336	0.470	0.838	1.000	1.000	0.561			
5b	26	4.9	2.587	0.150		0	1.61	1.079	3.264	0.417	0.838	1.000	1.000	0.498			
							2.01	0.808	4.511	0.312	0.822	1.000	1.000	0.380			
5c	26	4.9	5.047	0.150		0	1.61	1.162	6.368	0.230	0.838	1.000	1.000	0.274			
							2.01	0.946	8.800	0.188	0.822	1.000	1.000	0.229			
5d	26	4.9	12.179	0.150		0	1.61	1.204	15.367	0.099	0.838	1.000	1.000	0.118			
							2.01	0.878	21.235	0.072	0.822	1.000	1.000	0.088			
5e	26	4.9	12.179	0.150		0	1.61	1.528	15.367	0.125	0.838	1.000	1.000	0.137			
5f	26	4.9	12.179	0.150		0	1.61	1.528	15.367	0.125	0.838	1.000	1.000	0.125			
6a	27	6.3	2.217	0.225		0	1.61	1.087	2.797	0.490	0.772	1.000	1.000	0.635			
							2.01	0.841	3.866	0.379	0.745	1.000	1.000	0.509			
6b	27	6.3	4.909	0.225		0	1.61	1.043	6.194	0.212	0.772	1.000	1.000	0.275			
6c	27	6.3	9.280	0.225		0	1.61	1.180	11.710	0.127	0.772	1.000	1.000	0.165			
6d	27	6.3	9.280	0.225		0	1.61	1.358	11.710	0.147	0.772	1.000	0.160	0.168			
6e	27	6.3	9.280	0.225		0	1.61	1.593	11.710	0.172	0.772	1.000	0.164	0.172			
7a	28	8.6 to 10.4	4.535	0.096	2.078	0	0.80	0.773				1.000	1.000		-1.715	0.354	0.354
							0.90	1.094				1.000	1.000		-0.905	0.501	0.501
							0.92	1.152				1.000	1.000		-0.732	0.528	0.528
							0.94	1.283				1.000	1.000		-0.555	0.588	0.588
							0.96	1.604				1.000	1.000		-0.373	0.735	0.735
							0.98	1.954				1.000	1.000		-0.189	0.895	0.895
							1.00	2.103				1.000	1.000		0	0.963	0.963
							1.03	1.942				1.000	1.000		0.290	0.890	0.890

Table 2 (Contd.) - DETAILS OF HINGE MOMENT CORRELATION

No.	Ref.	$R \times 10^{-6}$	A	τ	$A\tau^{1/3}$	h/c	M	$-\frac{dC_H}{d\eta}$	$A\sqrt{M^2-1}$	$-\frac{1}{A}\frac{dC_H}{d\eta}$	K_ϕ	$k_{w(B)}$	K_x	$-\frac{1}{A}\left[\frac{dC_H}{d\eta}\right]''$	$\frac{M^2-1}{\tau^{2/3}}$	$-\tau^{1/3}\frac{dC_H}{d\eta}$	$-\tau^{1/3}\left[\frac{dC_H}{d\eta}\right]'$
7b	28	8.6 to 10.4	4.535			0	0.80	1.272				1.0	1.0		-1.715	0.583	0.583
							0.90	2.074				1.0	1.0		-0.905	0.950	0.950
							0.92	2.303				1.0	1.0		-0.732	1.055	1.055
							0.94	2.567				1.0	1.0		-0.555	1.176	1.176
							0.96	2.807				1.0	1.0		-0.373	1.286	1.286
							0.98	2.916				1.0	1.0		-0.189	1.336	1.336
							1.00	2.836				1.0	1.0		0	1.300	1.300
							1.03	2.636				1.0	1.0		0.209	1.208	1.208
8a	18	2.2 to 2.7	10.192	0.125	5.096	0.065	0.60	0.641				1.0	1.0		-2.560	0.321	0.321
							0.70	0.674				1.0	1.0		-2.040	0.337	0.337
							0.80	0.712				1.0	1.0		-1.440	0.356	0.356
							0.85	0.734				1.0	1.0		-1.110	0.367	0.367
							0.90	0.778				1.0	1.0		-0.743	0.389	0.389
							0.95	0.897				1.0	1.0		-0.390	0.448	0.448
							1.00	1.335				1.0	1.0		0	0.667	0.667
							1.05	1.557				1.0	1.0		0.410	0.778	0.778
							1.10	1.409				1.0	1.0		0.840	0.704	0.704
							1.18	1.357				1.0	1.0		1.570	0.678	0.678
8b	18	2.2 to 2.7	10.192	0.125	5.096	0.242	0.60	0.164				1.0	1.0		-2.560	0.082	0.082
							0.70	0.164				1.0	1.0		-2.040	0.082	0.082
							0.80	0.164				1.0	1.0		-1.440	0.082	0.082
							0.85	0.148				1.0	1.0		-1.110	0.074	0.074
							0.90	0.173				1.0	1.0		-0.743	0.087	0.087
							0.95	0.312				1.0	1.0		-0.390	0.156	0.156
							1.00	0.779				1.0	1.0		0	0.390	0.390
							1.05	0.822				1.0	1.0		0.410	0.411	0.411
							1.10	0.804				1.0	1.0		0.840	0.402	0.402
							1.18	-				1.0	1.0		1.570	-	-
8c	18	2.2 to 2.7	10.192	0.125	5.096	0.333	0.60	-0.047				1.0	1.0		-2.560	-0.023	-0.023
							0.70	-0.068				1.0	1.0		-2.040	-0.034	-0.034
							0.80	-0.123				1.0	1.0		-1.440	-0.061	-0.061
							0.85	-0.155				1.0	1.0		-1.110	-0.077	-0.077
							0.90	-0.113				1.0	1.0		-0.743	-0.056	-0.056
							0.95	0.047				1.0	1.0		-0.390	0.023	0.023
							1.00	0.321				1.0	1.0		0	0.160	0.160
							1.05	0.443				1.0	1.0		0.410	0.222	0.222
							1.10	0.417				1.0	1.0		0.840	0.209	0.209
							1.18	0.379				1.0	1.0		1.570	0.190	0.190
8d	18	2.2 to 2.7	10.192	0.125	5.096	0.441	0.60	-0.344				1.0	1.0		-2.560	-0.172	-0.172
							0.70	-0.371				1.0	1.0		-2.040	-0.185	-0.185
							0.80	-0.457				1.0	1.0		-1.440	-0.229	-0.229
							0.85	-0.526				1.0	1.0		-1.110	-0.263	-0.263
							0.90	-0.490				1.0	1.0		-0.743	-0.245	-0.245
							0.95	-0.331				1.0	1.0		-0.390	-0.166	-0.166
							1.00	0.086				1.0	1.0		0	0.043	0.043
							1.05	0.150				1.0	1.0		0.410	0.075	0.075
							1.10	0.179				1.0	1.0		0.840	0.089	0.089
							1.18	-				1.0	1.0		1.570	-	-

Table 2 (Contd.) - DETAILS OF HINGE MOMENT CORRELATION

No.	Ref.	$R \times 10^{-6}$	A	τ	$A\tau^{1/3}$	h/c	M	$-\frac{dC_H}{d\eta}$	$A\sqrt{M^2-1}$	$-\frac{1}{A}\frac{dC_H}{d\eta}$	K_ϕ	$k_{w(B)}$	K_x	$-\frac{1}{A}\left[\frac{dC_H}{d\eta}\right]''$	$\frac{M^2-1}{\tau^{2/3}}$	$-\tau^{1/3}\frac{dC_H}{d\eta}$	$-\tau^{1/3}\left[\frac{dC_H}{d\eta}\right]'$
8e	18	2.2 to 2.7	10.192	0.125	5.096	0.507	0.60	-0.504				1.0	1.0		-2.560	-0.252	-0.252
							0.70	-0.528				1.0	1.0		-2.040	-0.264	-0.264
							0.80	-0.612				1.0	1.0		-1.440	-0.306	-0.306
							0.85	-0.709				1.0	1.0		-1.110	-0.354	-0.354
							0.90	-0.709				1.0	1.0		-0.743	-0.354	-0.354
							0.95	-0.494				1.0	1.0		-0.390	-0.247	-0.247
							1.00	-0.021				1.0	1.0		0	-0.010	-0.010
							1.05	0.021				1.0	1.0		0.410	0.010	0.010
							1.10	0.042				1.0	1.0		0.840	0.021	0.021
							1.18	0.065				1.0	1.0		1.570	0.032	0.032
9a	29	6.1	2.047	0.128	1.033	0	1.40	0.907	2.005	0.443	0.851	0.897	0.935	0.621			
							1.80	0.778	3.063	0.380	0.854	0.956	0.978	0.475			
							2.20	0.640	4.011	0.313	0.839	0.974	0.983	0.390			
9b	30	10.5 to 13.5	2.047	0.128	1.033	0	0.60	0.413				0.937			-2.510	0.209	0.241
							0.90	0.498				0.937			-0.746	0.252	0.291
							0.94	0.556				0.937			-0.456	0.281	0.326
							0.96	0.625				0.937			-0.308	0.316	0.366
							0.98	0.756				0.937			-0.155	0.382	0.442
							1.00	0.951				0.937			0	0.481	0.557
							1.02	1.123				0.937			0.158	0.567	0.656
							1.04	1.077				0.937			0.319	0.544	0.630
							1.10	1.106				0.937			0.821	0.558	0.646
							1.19	1.129				0.937			1.633	0.570	0.660
							1.30	1.071				0.937			2.710	0.541	0.626
10a	31	12.5 to 19.4	2.978	0.087	1.318	0	1.30	1.134	2.473	0.382	0.880	0.930	0.962	0.485			
							1.50	1.020	3.329	0.343	0.898	0.960	0.979	0.407			
							1.65	0.974	3.908	0.328	0.902	0.970	0.982	0.382			
							1.80	0.905	4.456	0.304	0.901	0.977	0.984	0.355			
							2.00	0.837	5.157	0.281	0.895	0.984	0.986	0.324			
							0.50	0.458				0.938			-3.828	0.203	0.216
							0.70	0.481				0.938			-2.603	0.213	0.227
							0.90	0.837				0.938			-0.970	0.370	0.394
10b	32	12.5	2.978	0.087	1.318	0	0.90	0.688				0.938			-0.970	0.304	0.324
							0.94	1.215				0.938			-0.594	0.538	0.574
							0.96	1.432				0.938			-0.400	0.634	0.676
							0.98	1.157				0.938			-0.202	0.512	0.546
							1.00	1.392				0.938			0	0.616	0.657
							1.02	1.432				0.938			0.206	0.634	0.676
							1.04	1.553				0.938			0.417	0.687	0.732
							1.10	1.616				0.938			1.072	0.715	0.762
11	33	8.0	10.002	0.063	3.970	0	0.83	0.974				1.000			-2.000	0.386	0.386
							0.92	1.060				1.000			-1.000	0.421	0.421
							0.95	1.215				1.000			-0.619	0.482	0.482
12	34	5.8 to 15.0	10.341	0.161	5.627	0.400	1.10	0.525	4.739	0.051	0.818	0.978	0.902	0.070			
							1.20	0.453	6.859	0.044	0.820	0.990	0.943	0.057			
							1.30	0.399	8.590	0.039	0.823	0.994	0.967	0.050			

SYMBOLS

All symbols refer to controls unless otherwise specified.

A	aspect ratio, $= b^2/S$
b	net control span (see Fig. 2)
b_w	net wing span (see Fig. 2)
c	chord
c_r	root chord
$\bar{\bar{c}}$	aerodynamic mean chord, $= \int_0^b c^2 dy \Big/ \int_0^b c dy$
C_L	lift coefficient, = lift/qS (positive upwards)
C_m	pitching moment coefficient, = pitching moment/$qS\bar{\bar{c}}$ (positive nose up)
C_H	hinge moment coefficient, = hinge moment/$qS\bar{\bar{c}}$ (positive when it tends to deflect the trailing edge downwards)
$\frac{dC_H}{d\eta}$	derivative of C_H with respect to η at $\eta = 0$
$\left[\frac{dC_H}{d\eta}\right]'$	$= \frac{1}{k_{w(B)}} \times \frac{dC_H}{d\eta}$
$\left[\frac{dC_H}{d\eta}\right]''$	$= \frac{1}{k_{w(B)}} \times \frac{1}{K_x} \times \frac{1}{K_\phi} \times \frac{dC_H}{d\eta}$
C_p	pressure coefficient $= \frac{p-p_o}{q}$
C_1, C_2, C_3	constants in the Busemann third order approximation for the pressure coefficient in two dimensional isentropic supersonic flow
g	width of gap between wing and body of wing-body combinations
H	hinge moment (positive when it tends to deflect the trailing edge downwards)
h	chordwise location of control hinge line, measured aft from control leading edge
K_ϕ	control hinge moment thickness factor at supersonic speeds

$$= \frac{\left[\frac{dC_H}{d\eta}\right] \text{ third order two dimensional approximation}}{\left[\frac{dC_H}{d\eta}\right] \text{ linear theory two dimensional approximation}}$$

$$= 1 - \frac{C_2}{C_1}\phi + \frac{3}{4}\frac{C_3}{C_1}\phi^2$$

SYMBOLS (Contd.)

$k_{w(B)}$ the ratio of the lift on a control in the presence of a circular cross-section body to the lift on an isolated control (of aspect ratio twice that of the exposed panel), lift produced by control deflection with the body at zero incidence (see Ref.8)

K_x factor for body interference on aerodynamic centre position of rectangular controls at supersonic speeds

$$= \frac{\left(\frac{x_a}{c}\right)_{\text{control + body}} - \frac{h}{c}}{\left(\frac{x_a}{c}\right)_{\text{control}} - \frac{h}{c}}$$

K_g control hinge moment gap factor

$$= \frac{\left[\text{lift or hinge moment on wing or control}\right]\ g \neq 0}{\left[\text{lift or hinge moment on wing or control}\right]\ g = 0}$$

K_{τ_1} control hinge moment trailing edge thickness factor at transonic speeds

$$= \frac{\left[\frac{dC_H}{d\eta}\right]_{\tau_1 \neq 0}}{\left[\frac{dC_H}{d\eta}\right]_{\tau_1 = 0}}$$

M Mach number

M' first moment of area of the control behind the hinge line about the hinge line

p static pressure

q kinetic pressure

R Reynolds number based on wing root chord

r body radius

S plan area

s gross semi-span of control mounted on body (= b/2 + r)

s_w gross semi-span of wing (= $b_w/2 + r$)

t_w wing thickness

t control thickness at leading edge

t_1 control thickness at trailing edge

x chordwise distance

x_a chordwise location of aerodynamic centre

y spanwise distance

SYMBOLS (Contd.)

y_c	distance from wing-body junction or wing centre line (configuration without body) to inboard edge of control (see Fig. 2)
α	incidence
β	$\sqrt{M^2-1}$
γ	ratio of specific heats
$(\delta^*_{turb})_{mean}$	mean value across the control span of the displacement thickness of a flat plate boundary layer, with transition at the wing leading edge
η	control deflection (radians), measured normal to the hinge line, positive when the trailing edge is deflected downwards
λ	taper ratio
$\Lambda_{H.L.}$	sweepback of hinge line (degrees)
$\Lambda_{L.E.}$	leading edge sweepback (degrees)
Λ_T	tip sweepback of controls with raked tips (degrees)
τ	control thickness parameter = t/c
τ_1	control trailing edge thickness parameter = t_1/c
ϕ	trailing edge included angle, defined as $2 \tan^{-1} \frac{1}{2}(\tau - \tau_1)$
θ	deflection angle in two dimensional supersonic flow, positive for a compression and negative for an expansion

Suffices

w	refers to the net wing
o	refers to free stream conditions
1	refers to conditions at control trailing edge

REFERENCES

No.	Author	Title, etc.
1	C.J. Donlan B.C.I. Myers A.T. Mattson	A comparison of the aerodynamic characteristics at transonic speeds of four wing-fuselage configuration as determined from different test techniques. ARC 13956, April 1951
2	K.R. Czarnecki J.N. Mueller	Investigation at supersonic speeds of some of the factors affecting the flow over a rectangular wing with symmetrical circular-arc section and 30% chord trailing edge flap. NACA RM L50J18 (TIB2599), January 1951
3	I.H. Abbott A.E. von Doenhoff	Theory of wing sections, including a summary of airfoil data. Revd. ed. Dover Publications 1959
4	P.A. Lagerstrom M.E. Graham	Low aspect ratio rectangular wings in supersonic flow. Douglas Aircraft Rept. No.SM-13110, December 1947
5	W.A. Tucker R.L. Nelson	Theoretical characteristics in supersonic flow of constant-chord partial-span control surfaces on rectangular wings having finite thickness. NACA TN 1708, September 1948
6	E.A. Bonney	Engineering Supersonic Aerodynamics. McGraw Hill 1950, pp.76, 77
7	K.G. Winter C.S. Brown	Supersonic wind tunnel tests on guided weapon control surfaces mounted on a body. 3 tests of three rectangular controls at Mach numbers of 1.61, 2.00 and 2.48. Unpublished M.O.A. Report
8	W.C. Pitts J.N. Nielsen G.E. Kaattari	Lift and centre of pressure position of wing-body-tail combinations at subsonic, transonic and supersonic speeds. NACA Rept. 1307, 1957

REFERENCES (Contd.)

No.	Author	Title, etc.
9	D.W. Dugan K. Hikido	Theoretical investigation of the effects upon lift of a gap between wing and body of a slender wing-body combination. NACA TN 3224, August 1954
10	D.W. Dugan	Experimental investigation of some aerodynamic effects of a gap between wing and body of a moderately slender wing-body combination at a Mach number of 1.4. NACA RM A55D08 (TIB 4687), May 1955
11	T. Von Karman	The similarity law of transonic flow. Jour. Math. and Phys., Vol. XXVI, No. 3, October 1947, pp. 182-190
12	J.R. Spreiter	Similarity laws for transonic flow about wings of finite span. ARC 13968, April 1951
13	J.R. Spreiter	On the application of transonic similarity rules to wings of finite span. NACA Rept. 1153, 1953
14	A. Busemann	Application of transonic similarity. NACA TN 2687, April 1952
15	K.C. Harder	Transonic similarity rules for lifting wings. NACA TN 2724, June 1952
16	J.B. McDevitt	A correlation by means of the transonic similarity rules of the experimentally determined characteristics of 22 rectangular wings of symmetrical profile. ARC 16048, July 1953
17	D. Kuchemann	A simple method of calculating the span and chord-wise loadings on straight and swept wings of any given aspect ratio at subsonic speeds. ARC R&M 2935, August 1952

REFERENCES (Contd.)

No.	Author	Title, etc.
18	R.F. Thompson	Hinge-moment, lift, and pitching-moment characteristics of a flap-type control surface having various hinge line locations on a 4 per cent thick 60^{o} delta wing, Transonic-bump method. NACA RM L54B08 (TIB 4166), March 1954
19	L.D. Guy	Effects of overhang balance on the hinge moment and effectiveness characteristics of an unswept trailing edge control on a 60^{o} delta wing at transonic and supersonic speeds. NACA RM L54G12a (TIB 4390), September 1954
20	G. Guderley H. Yoshihara	The flow over a wedge profile at Mach number 1. Journal Aero. Sci. Vol.17, pp.723-735
21	W.G. Vincenti C.B. Wagoner	Transonic flow past a wedge profile with detached bow wave. NACA Rept 1095, 1952
22	W.G. Vincenti	Measurements of the effects of finite span on the pressure distribution over double wedge wings at Mach numbers near shock attachment. NACA TN 3522, September 1955
23	L.D. Guy	Hinge moment and effectiveness of an unswept constant-chord control and an overhang-balanced, swept hinge-line control on an 80^{o} swept pointed wing at Mach numbers from 0.75 to 1.96. NACA RM L56F11 (TIL 5211), August 1956
24	J.W. Boyd F.A. Pfyl	Experimental investigation of aerodynamically balanced trailing edge control surfaces on an aspect ratio 2 triangular wing at subsonic and supersonic speeds. NACA RM A52L04 (TIB 3610), February 1953
25	J.W. Boyd	Aerodynamic characteristics of two 25 per cent area trailing-edge flaps on an aspect ratio 2 triangular wing at subsonic and supersonic speeds. NACA RM A52D01c (TIB 3260), July 1952

REFERENCES (Contd.)

No.	Author	Title, etc.
26	D.R. Lord K.R. Czarnecki	Aerodynamic characteristics of several flap-type trailing-edge controls on a trapezoidal wing at Mach numbers of 1.61 and 2.01. NACA RM L54D19 (TIB 4255), June 1954
27	D.R. Lord K.R. Czarnecki	Hinge-moment characteristics for a series of controls and balancing devices on a 60° delta wing at Mach numbers of 1.61 and 2.01. NACA RM L57B01 (TIL 5489), April 1957
28	C.F. Whitcomb C.C. Critzos	Transonic characteristics of outboard ailerons on a 4-per cent-thick 30° sweptback wing, including some effects of aileron trailing-edge thickness and aerodynamic balance. NACA RM L58E05 (TIL 6050), July 1958
29	D. Isaacs	Tests at subsonic and supersonic speeds on a slender cambered wing with fin, underwing engine nacelles and trailing edge controls. Unpublished M.O.A. Report
30	T.E. Bateman G.T. Downer	Force and pressure measurements on a supersonic transport model in the A.R.A. transonic tunnel. Unpublished A.R.A. Note
31	G.F. Moss	Unpublished RAE wind tunnel tests.
32	P.G. Hutton D. Morton	Results of pressure plotting and control hinge moment tests on 1/9th scale model of Fairy delta 2 in the A.R.A. transonic tunnel. A.R.A. Model Test Note J.12/1, May 1961
33	J.D. Stephenson A.R. Amuedo	Tests of a triangular wing of aspect ratio 2 in the Ames 12-foot pressure wind tunnel. II - the effectiveness and hinge moments of a constant-chord plain flap. NACA RM A8E03 (TIB 1916), September 1948
34	C.W. Martz J.W. Goslee	Rocket model investigation to determine the hinge-moment and normal-force properties of a full-span, constant-chord, partially balanced trailing-edge control on a 60° clipped delta wing between Mach numbers of 0.50 and 1.26. NACA RM L53I04 (TIB 3943), October 1953

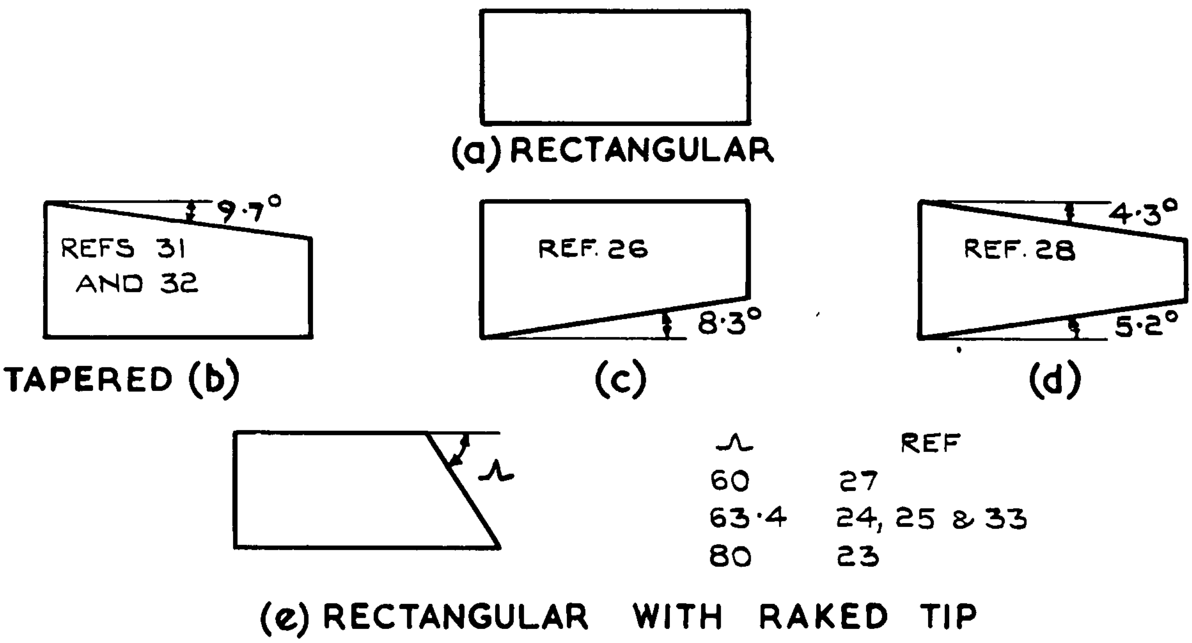

FIG. 1 TYPES OF CONTROL PLANFORM

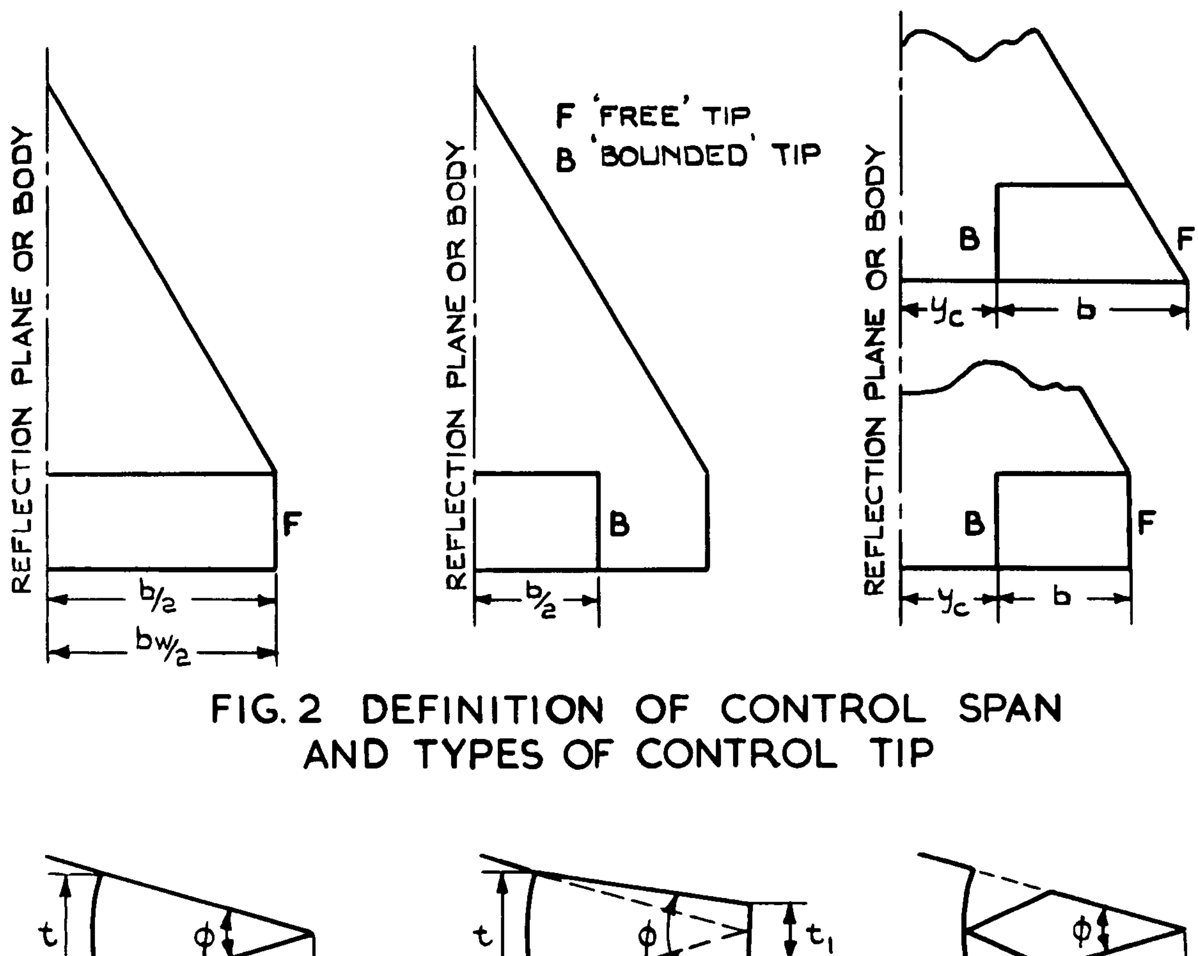

FIG. 2 DEFINITION OF CONTROL SPAN AND TYPES OF CONTROL TIP

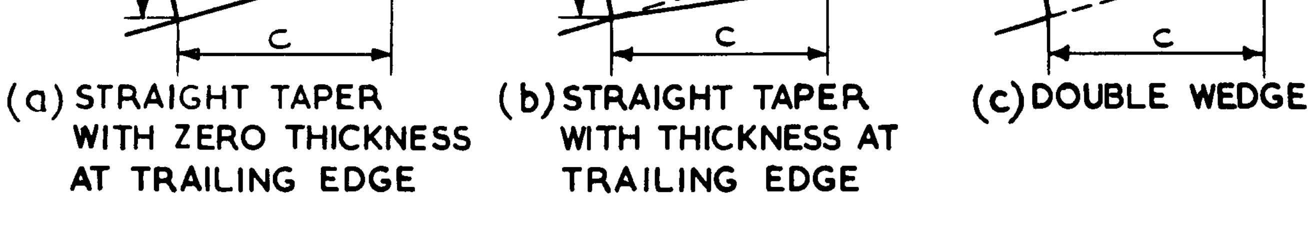

FIG. 3 TYPES OF CONTROL CROSS SECTION

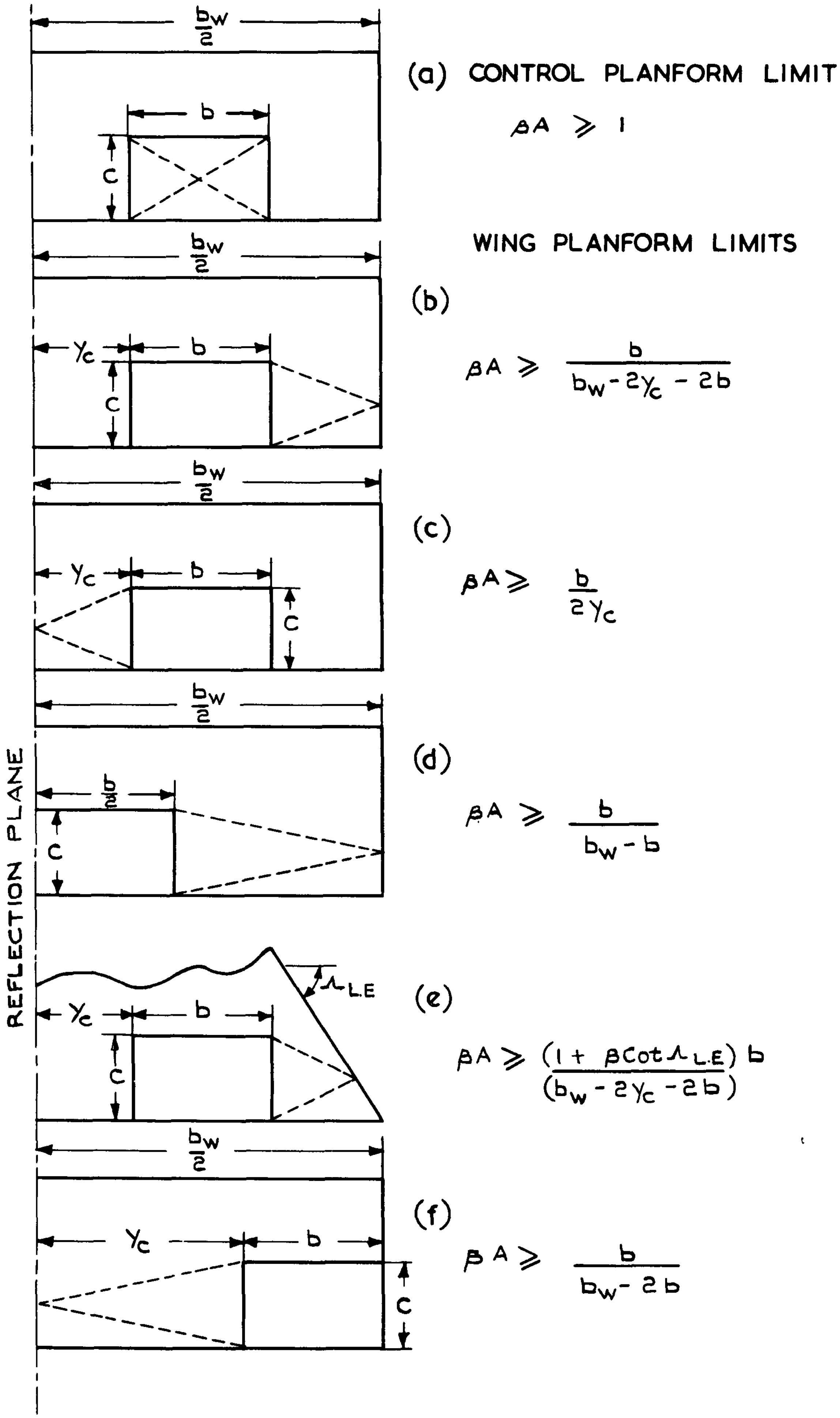

FIG. 4 MACH LINE LOCATION AT LOWER LIMIT OF APPLICABILITY OF PRESENT SUPERSONIC LINEAR THEORY EXPRESSIONS FOR $\frac{dC_H}{d\eta}$

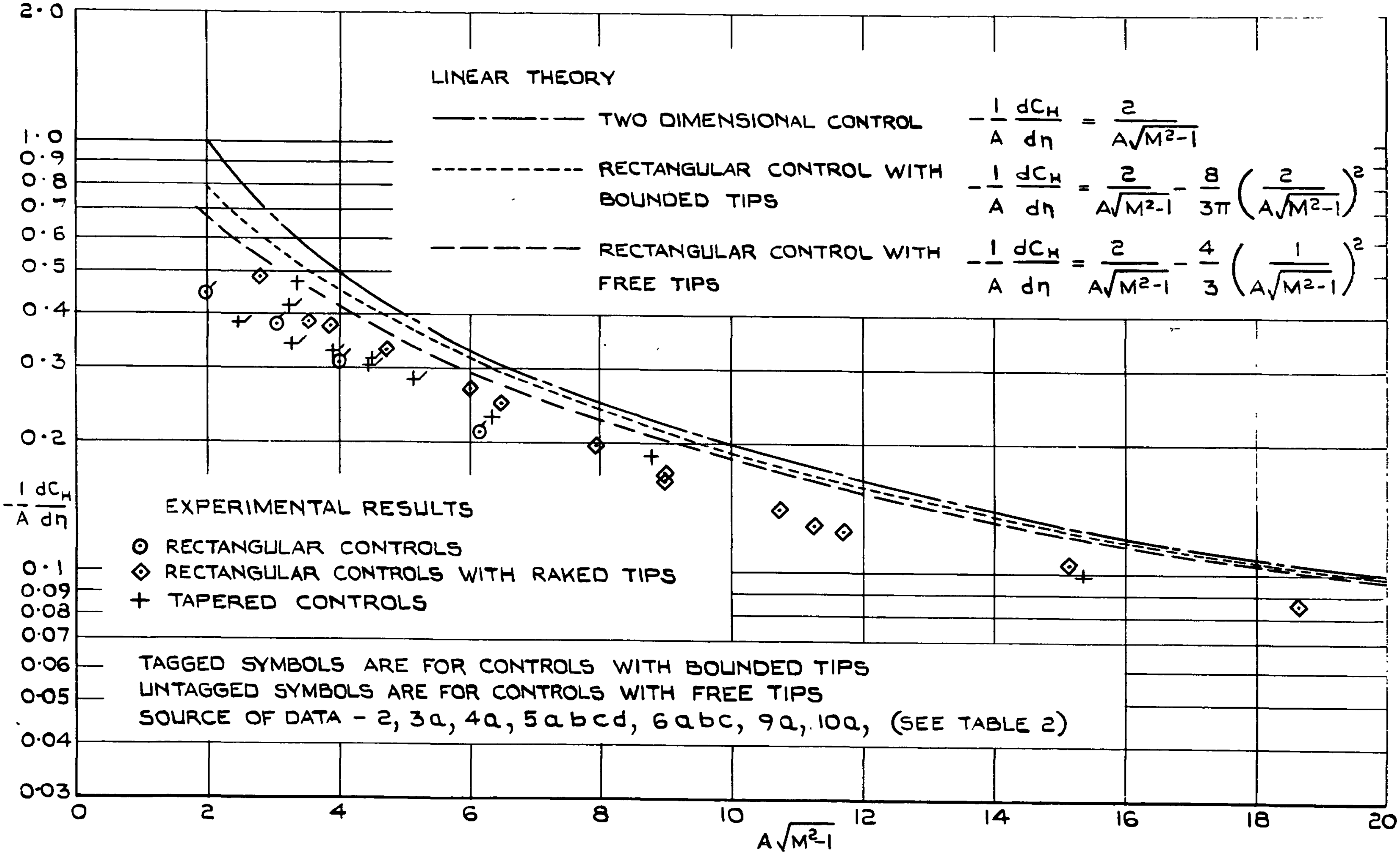

FIG. 5 VARIATION OF $-\frac{1}{A}\frac{dC_H}{d\eta}$ WITH $A\sqrt{M^2-1}$ AT SUPERSONIC SPEEDS

(HINGE LINE AT CONTROL LEADING EDGE)

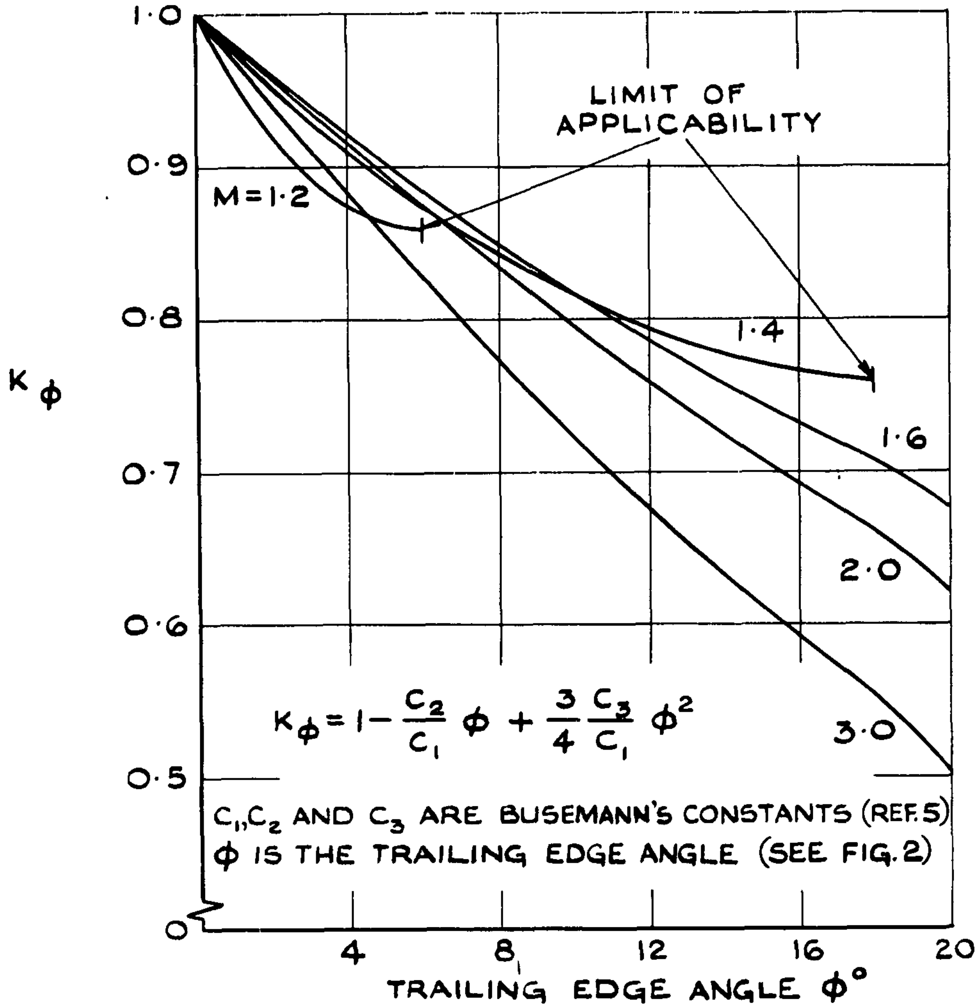

FIG. 6. THICKNESS FACTOR FOR TRAILING EDGE CONTROLS AT SUPERSONIC SPEEDS

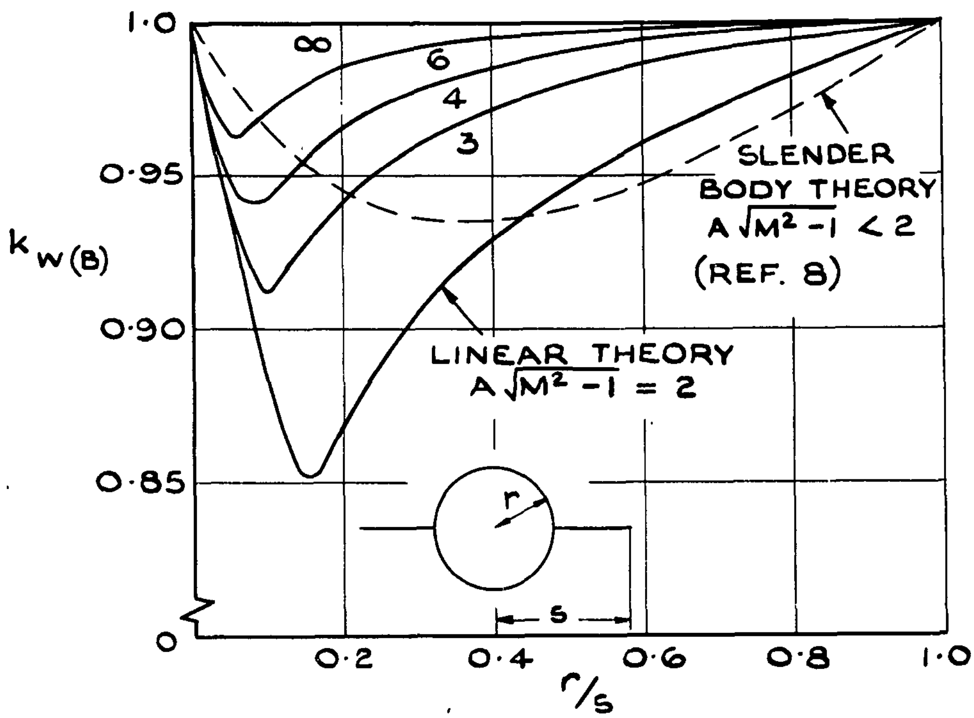

FIG. 7. FACTOR FOR BODY INTERFERENCE ON LIFT OF RECTANGULAR CONTROLS AT SUPERSONIC SPEEDS

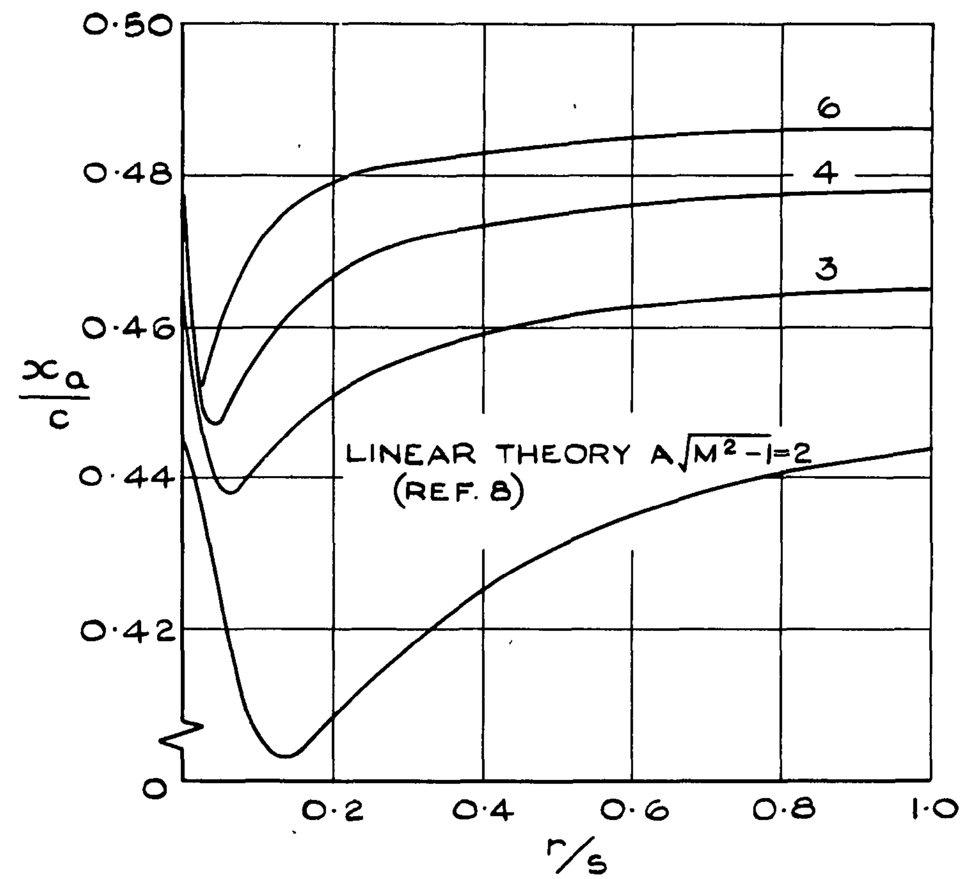

FIG.8 EFFECT OF BODY INTERFERENCE ON AERODYNAMIC CENTRE OF RECTANGULAR CONTROLS AT SUPERSONIC SPEEDS

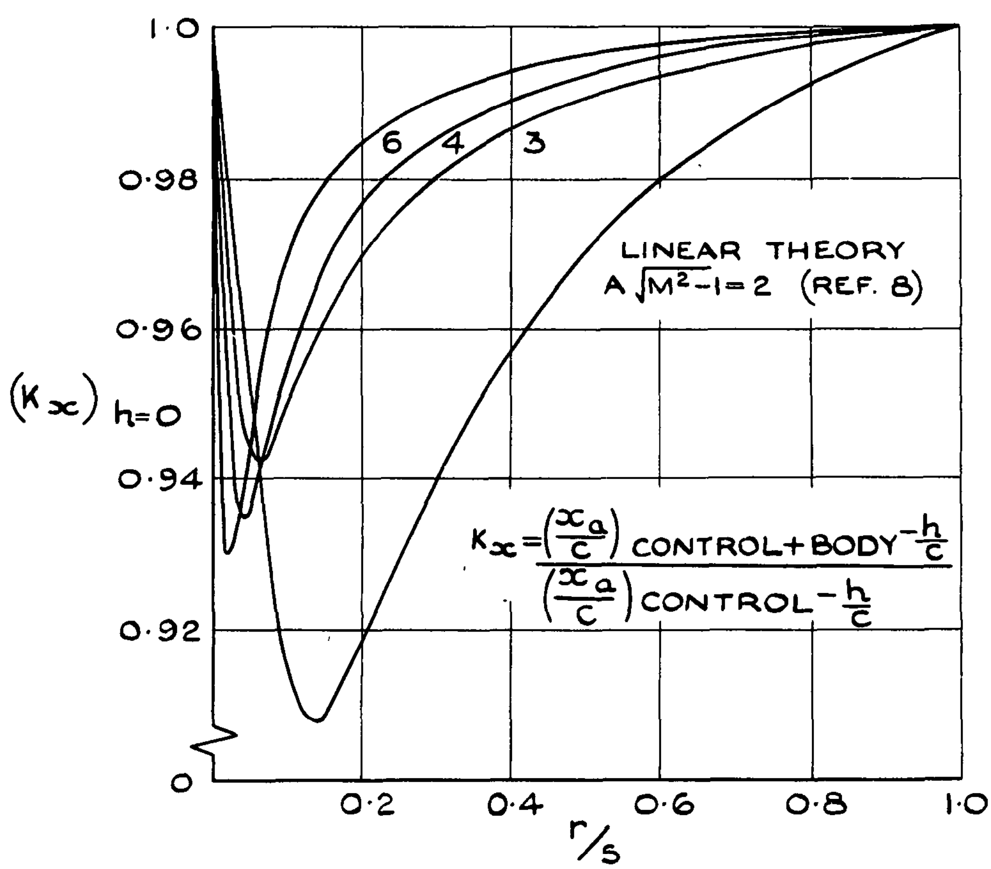

FIG.9 FACTOR FOR BODY INTERFERENCE ON AERODYNAMIC CENTRE OF RECTANGULAR CONTROLS AT SUPERSONIC SPEEDS (CONTROL HINGE LINE AT LEADING EDGE)

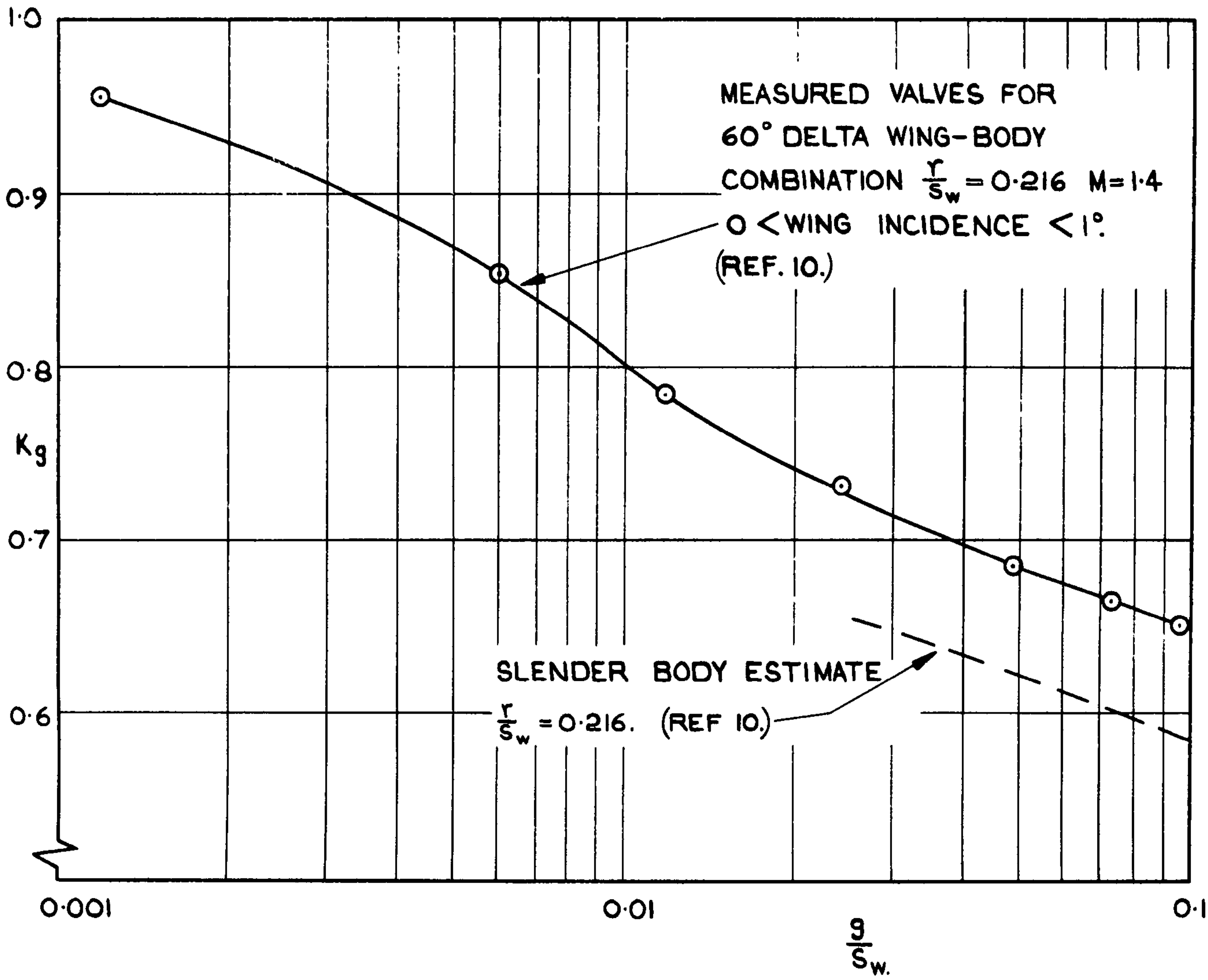

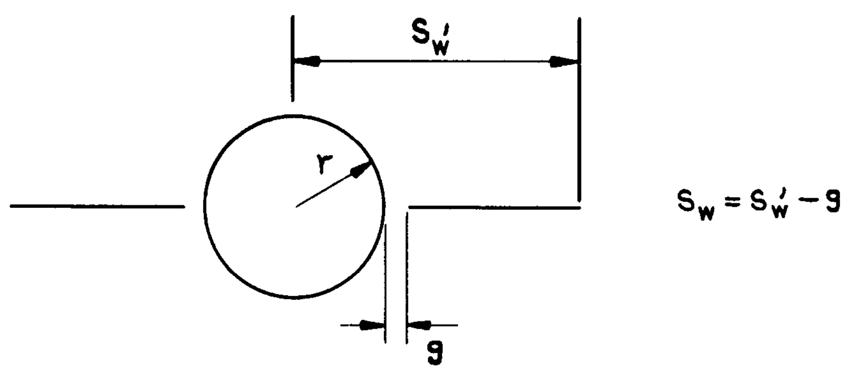

$$K_g = \frac{(\text{LIFT ON WING})\quad g \neq 0}{(\text{LIFT ON WING})\quad g = 0.}$$

BODY IS AT ZERO INCIDENCE AND LIFT IS OBTAINED BY WING INCIDENCE ONLY.

FIG. 10 GAP FACTOR FOR THE LIFT ON THE WINGS OF A WING-BODY COMBINATION.

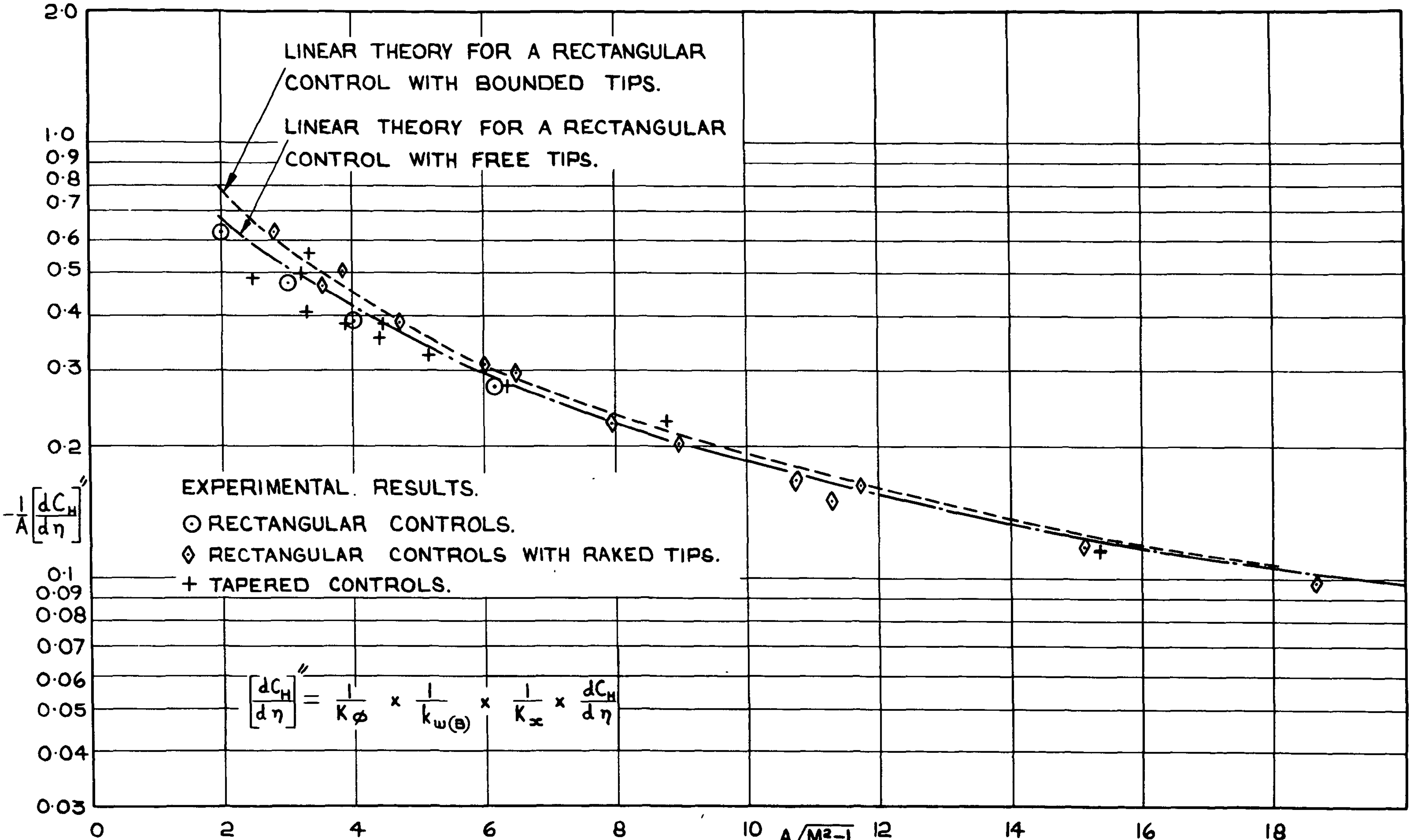

FIG.11 VARIATION OF $-\frac{1}{A}\left[\frac{dC_H}{d\eta}\right]''$ WITH $A\sqrt{M^2-1}$ AT SUPERSONIC SPEEDS.

(HINGE LINE AT CONTROL LEADING EDGE.)

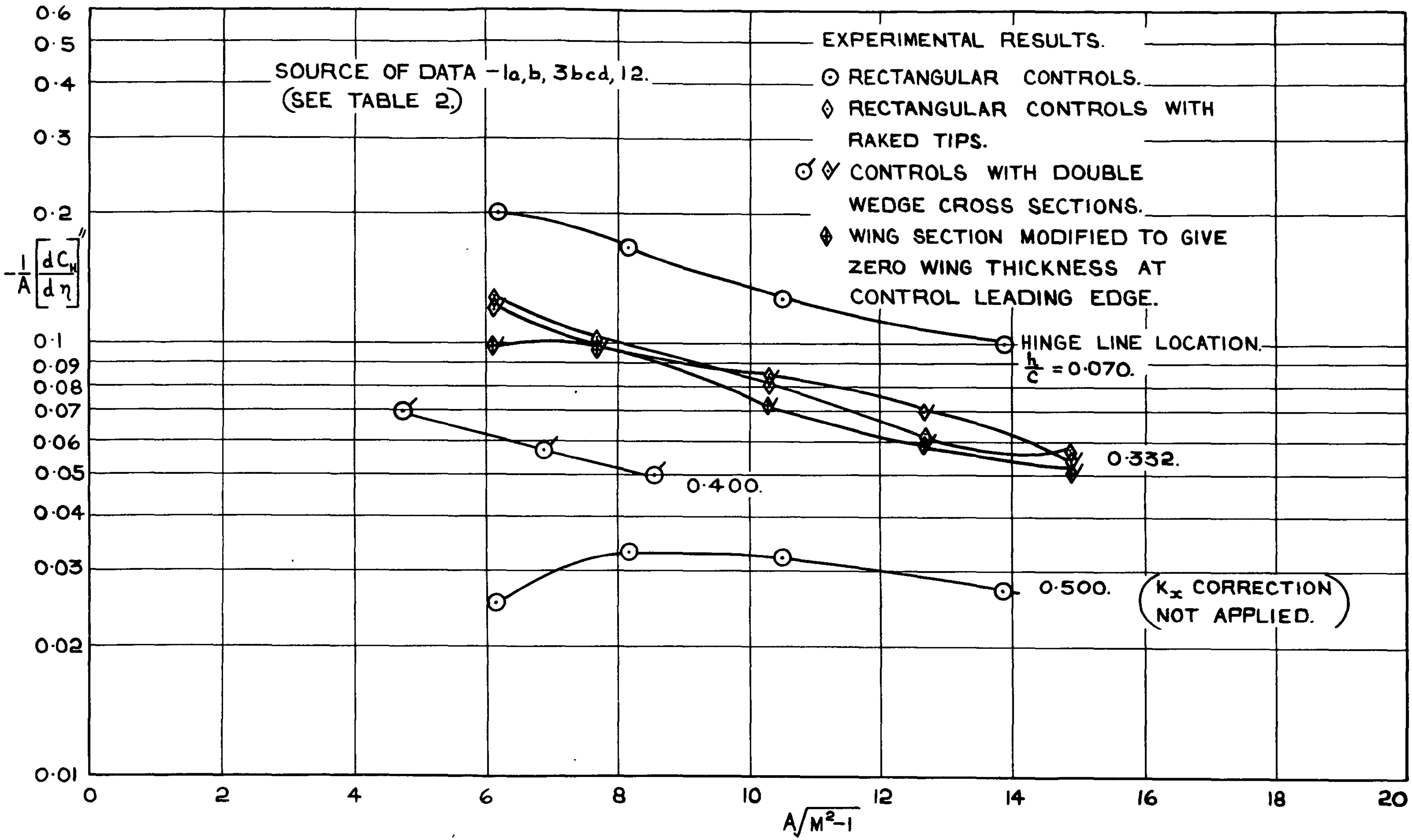

FIG. 12 EFFECT OF HINGE LINE LOCATION ON THE VARIATION OF $-\frac{1}{A}\left[\frac{dC_H}{d\eta}\right]''$ WITH $A\sqrt{M^2-1}$ AT SUPERSONIC SPEEDS.

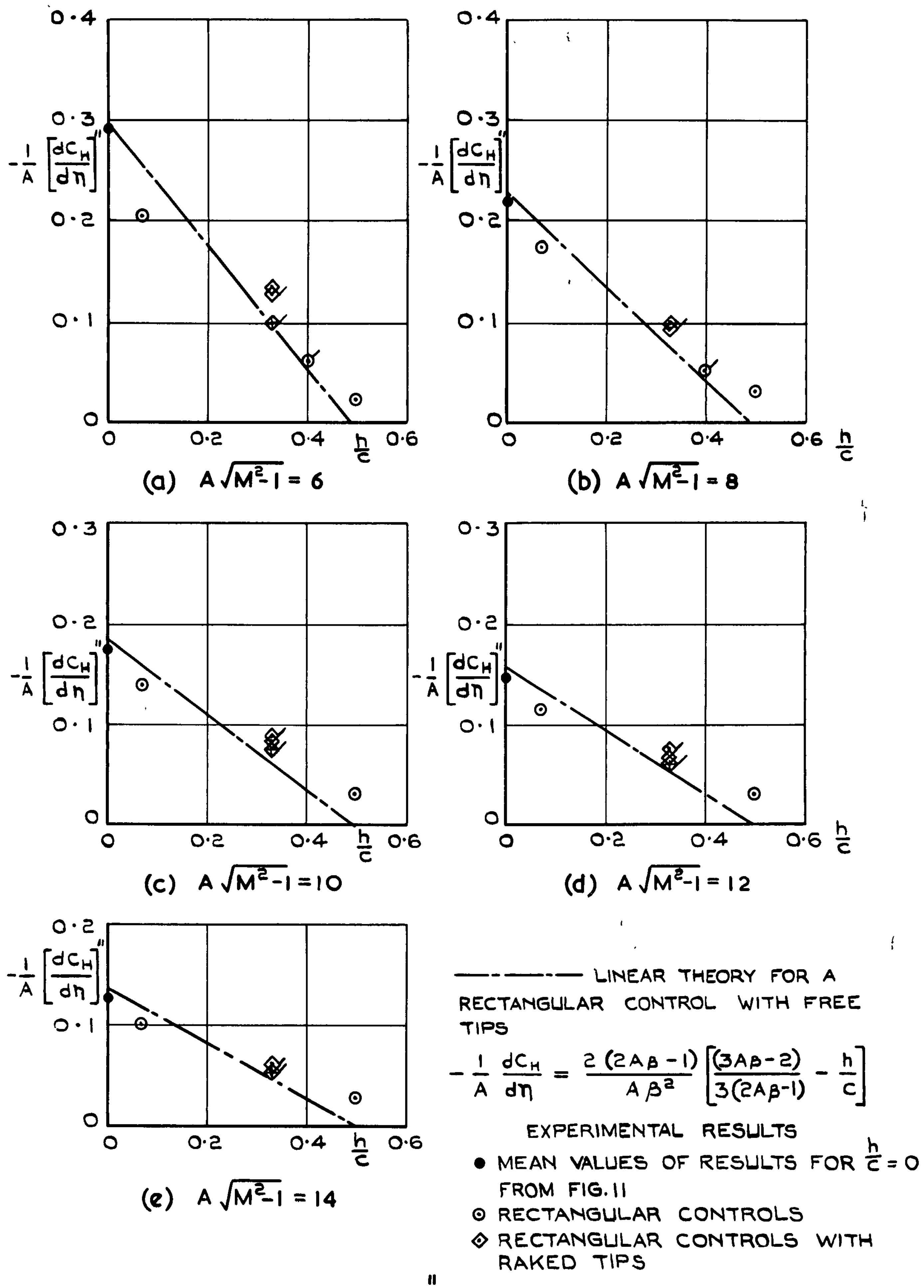

FIG. 13 VARIATION OF $-\frac{1}{A}\left[\frac{dC_H}{d\eta}\right]''$ WITH $\frac{h}{c}$ AT SUPERSONIC SPEEDS

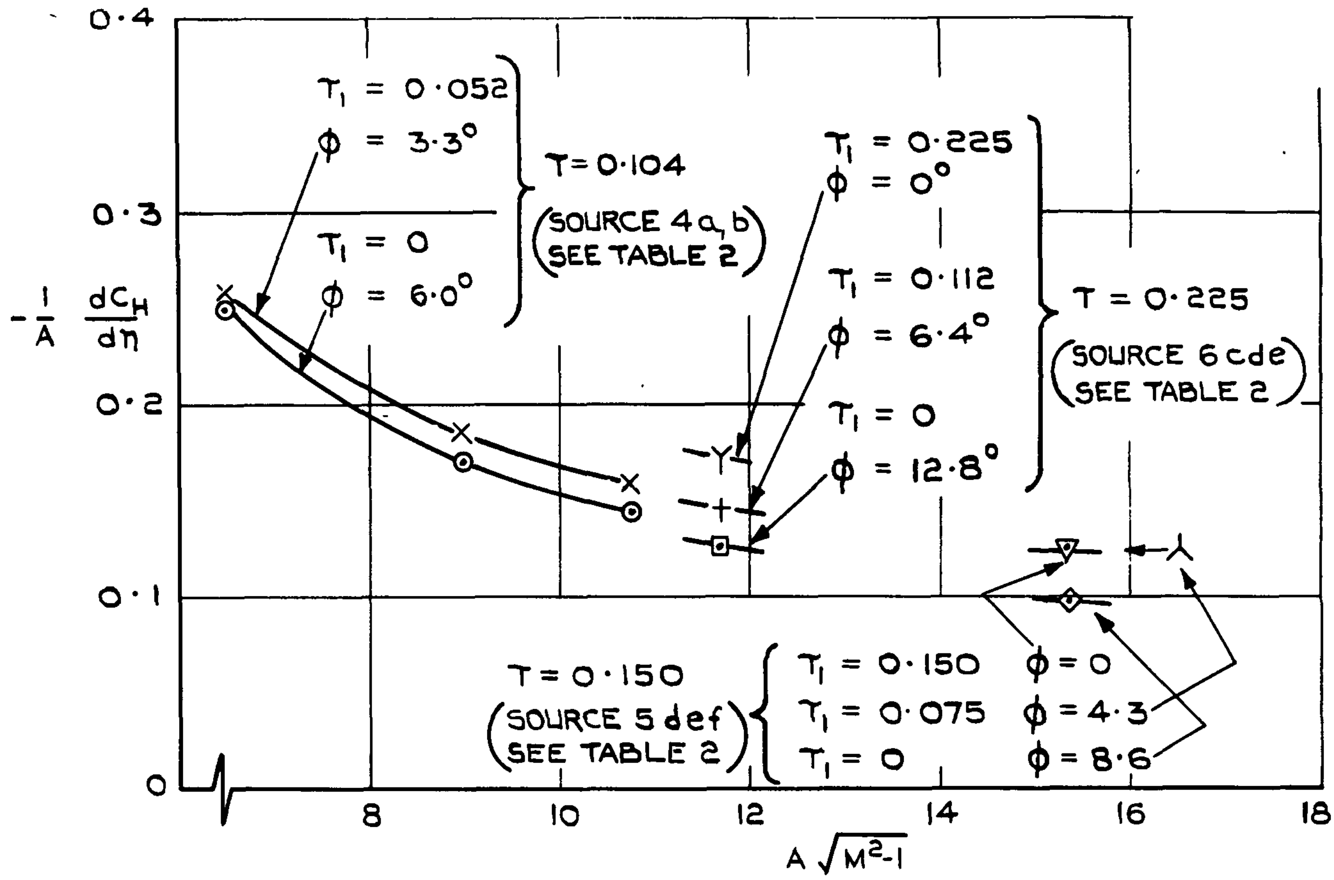

(a) $\frac{dC_H}{d\eta}$ UNCORRECTED FOR TRAILING EDGE ANGLE

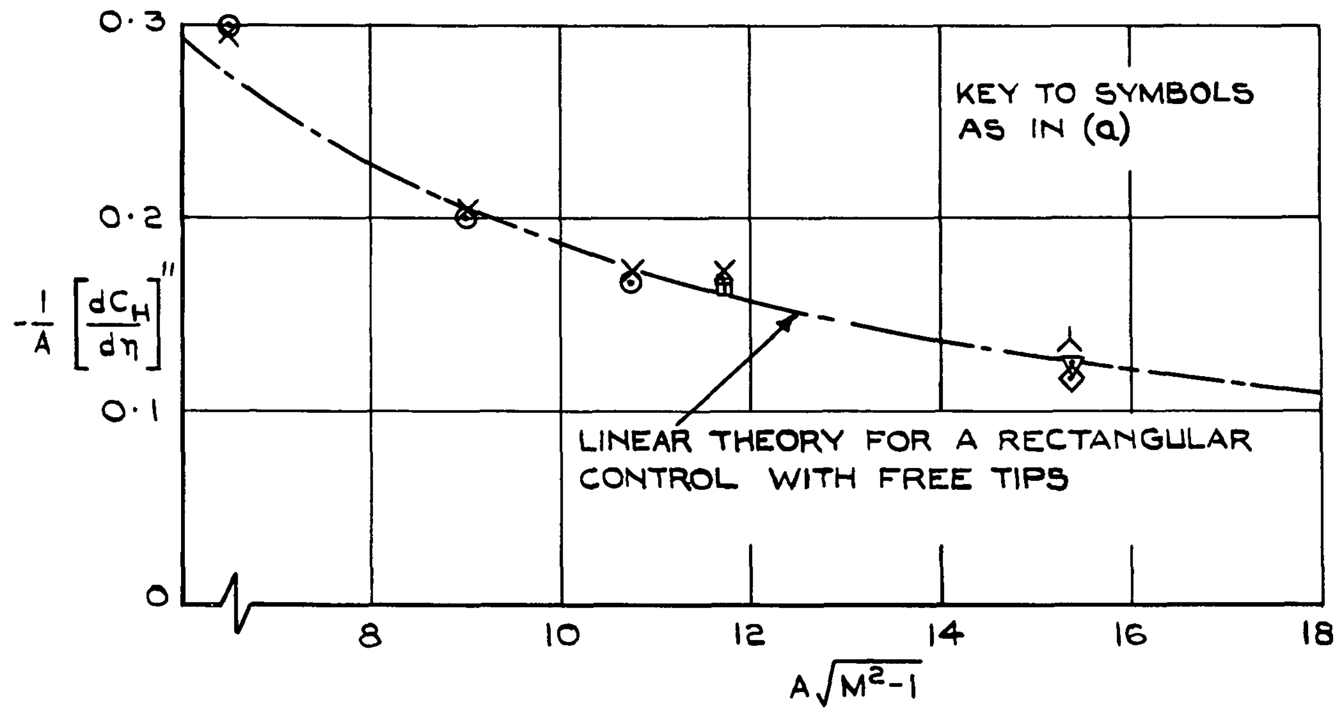

(b) $\frac{dC_H}{d\eta}$ CORRECTED FOR TRAILING EDGE ANGLE

FIG. 14 EFFECT OF TRAILING EDGE THICKNESS ON $\frac{dC_H}{d\eta}$ AT SUPERSONIC SPEEDS

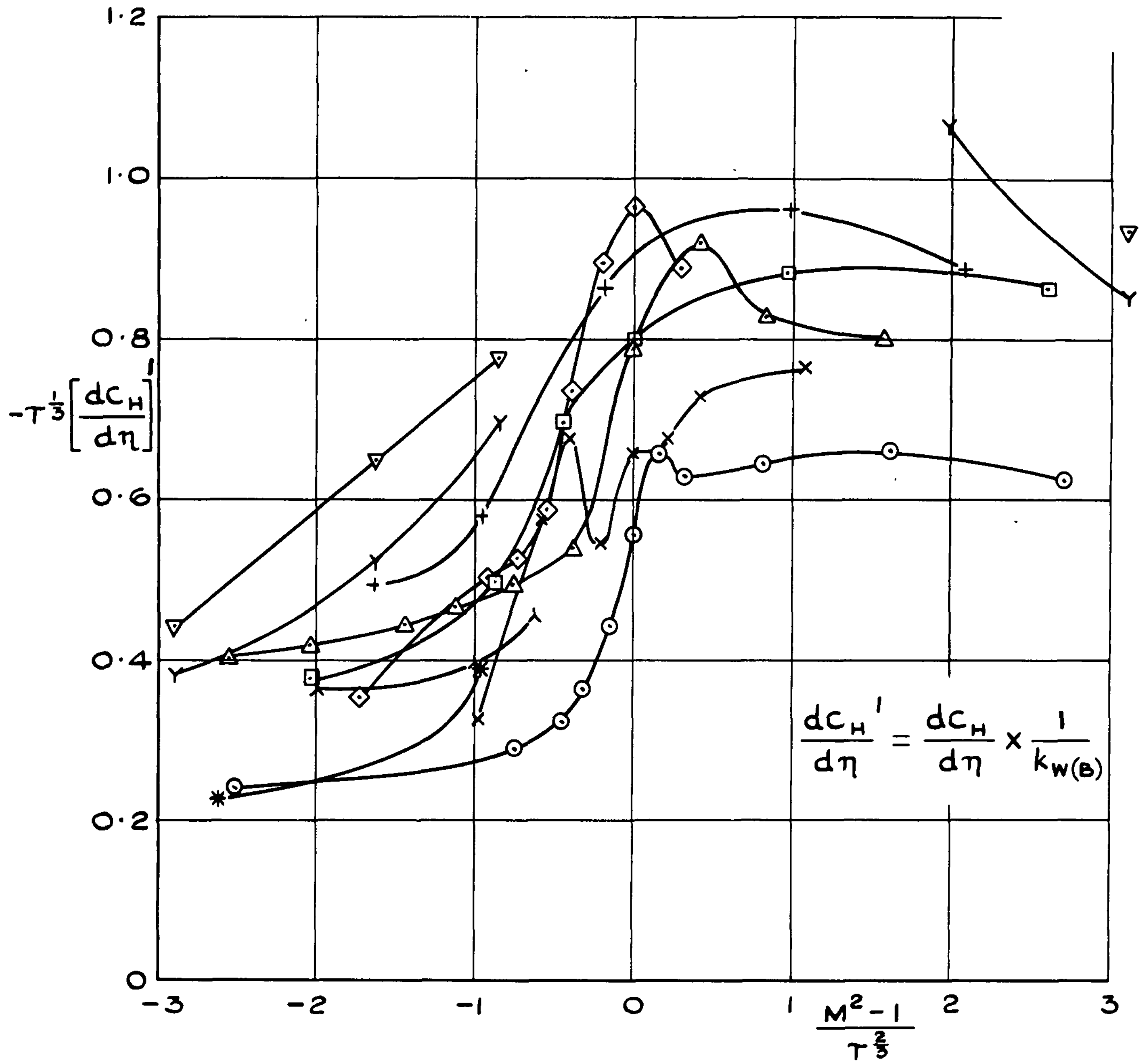

	SOURCE OF DATA (SEE TABLE 2)	A	τ	$A\tau^{\frac{1}{3}}$
+	1a AND b ✳	8·233	0·133	4·201
⊡	2	4·717	0·100	2·189
Y	3a	13·584	0·104	6·389
▽	4a	7·817	0·104	3·676
◇	7a	4·535	0·096	2·078
△	8 a,b,c,d,e ✳	10·192	0·125	5·096
⊙	9b	2·047	0·128	1·033
✱	10a	2·978	0·087	1·318
×	10b	2·978	0·087	1·318
⅄	11	10·002	0·063	3·970

✳ RESULTS EXTRAPOLATED TO ZERO h/c

FIG.15. VARIATION OF $-\tau^{\frac{1}{3}}\left[\frac{dC_H}{d\eta}\right]'$ WITH $\frac{M^2-1}{\tau^{\frac{2}{3}}}$ AT TRANSONIC SPEEDS

(HINGE LINE AT CONTROL LEADING EDGE)

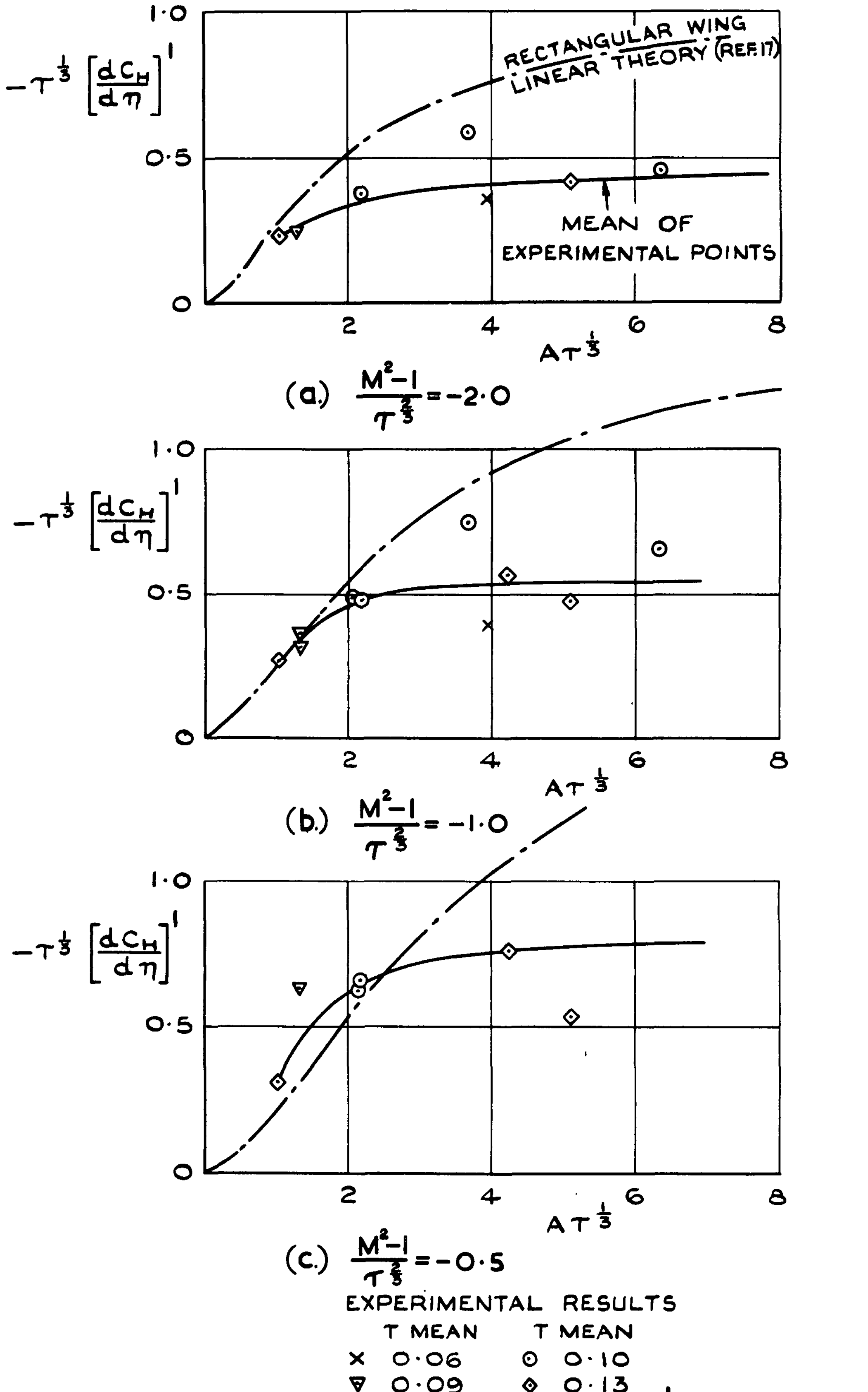

FIG.16. VARIATION OF $-\tau^{\frac{1}{3}}\left[\frac{dC_H}{d\eta}\right]^1$ WITH $A\tau^{\frac{1}{3}}$ AT TRANSONIC SPEEDS

(HINGE LINE AT CONTROL LEADING EDGE)

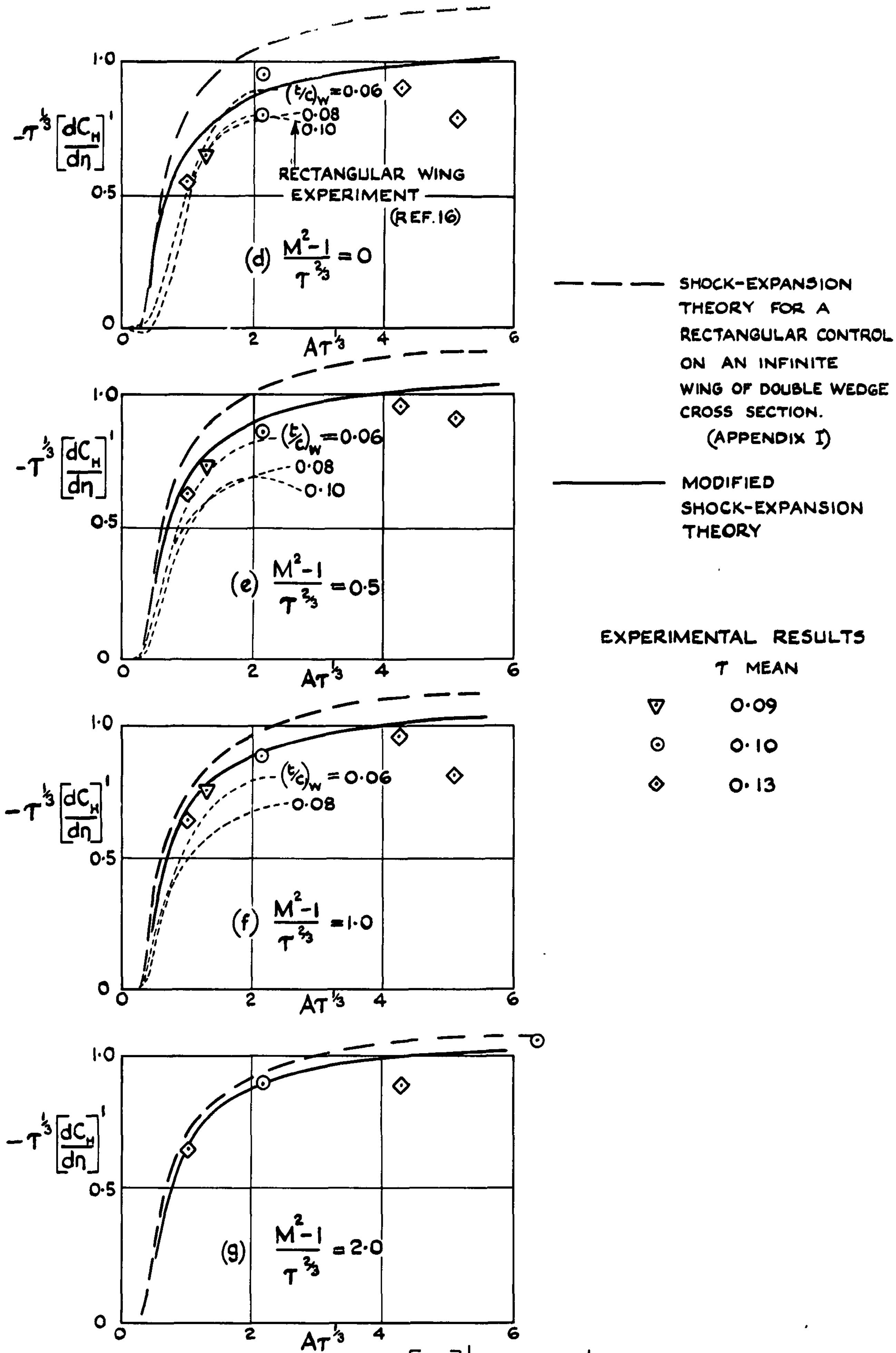

FIG.16 (CONCLD.) VARIATION OF $-\tau^{\frac{1}{3}}\left[\frac{dC_H}{d\eta}\right]'$ WITH $A\tau^{\frac{1}{3}}$ AT TRANSONIC SPEEDS.
(HINGE LINE AT CONTROL LEADING EDGE)

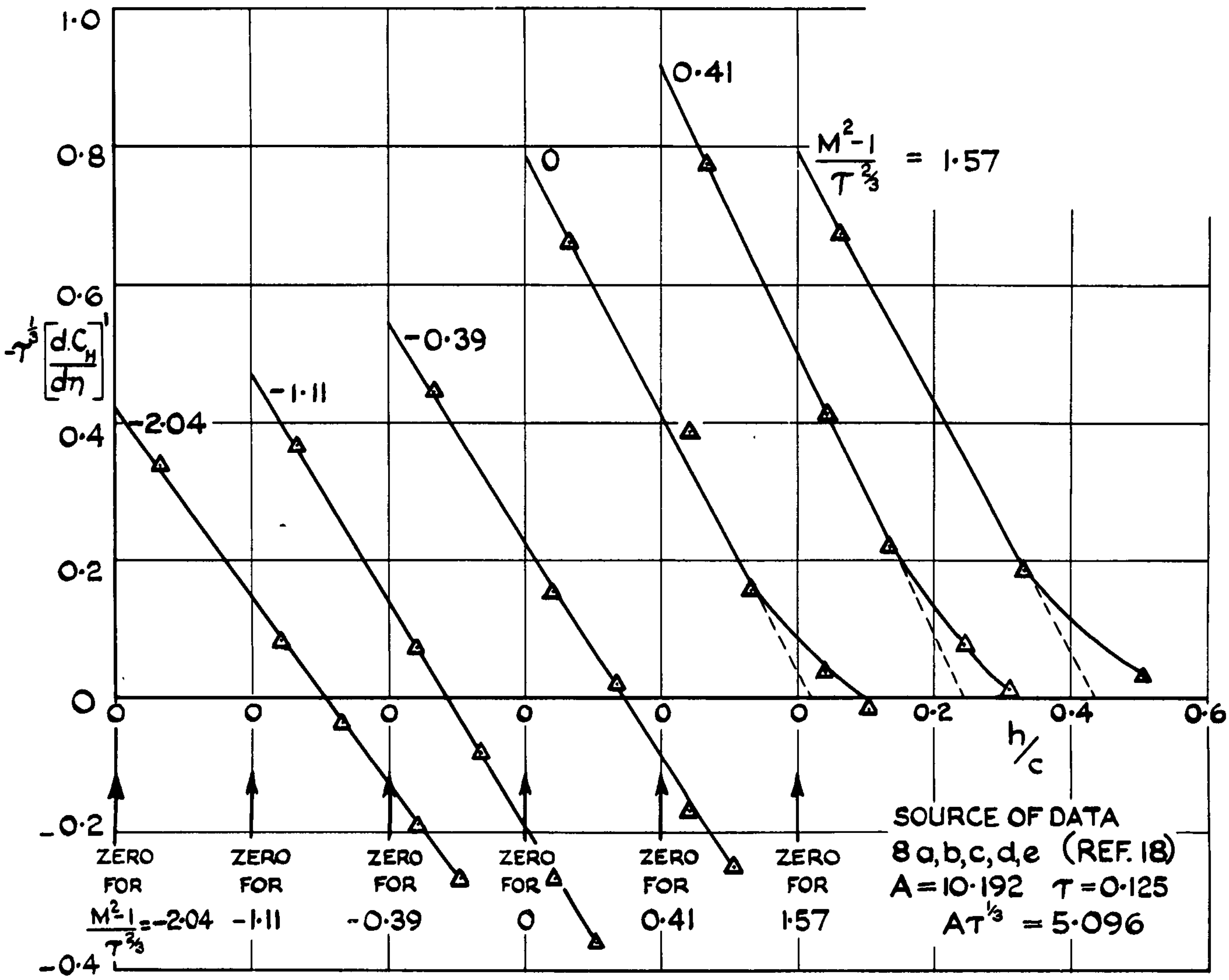

FIG. 17 VARIATION OF $-\tau^{\frac{1}{3}}\left[\frac{dC_H}{d\eta}\right]'$ WITH $\frac{h}{c}$ AT TRANSONIC SPEEDS.

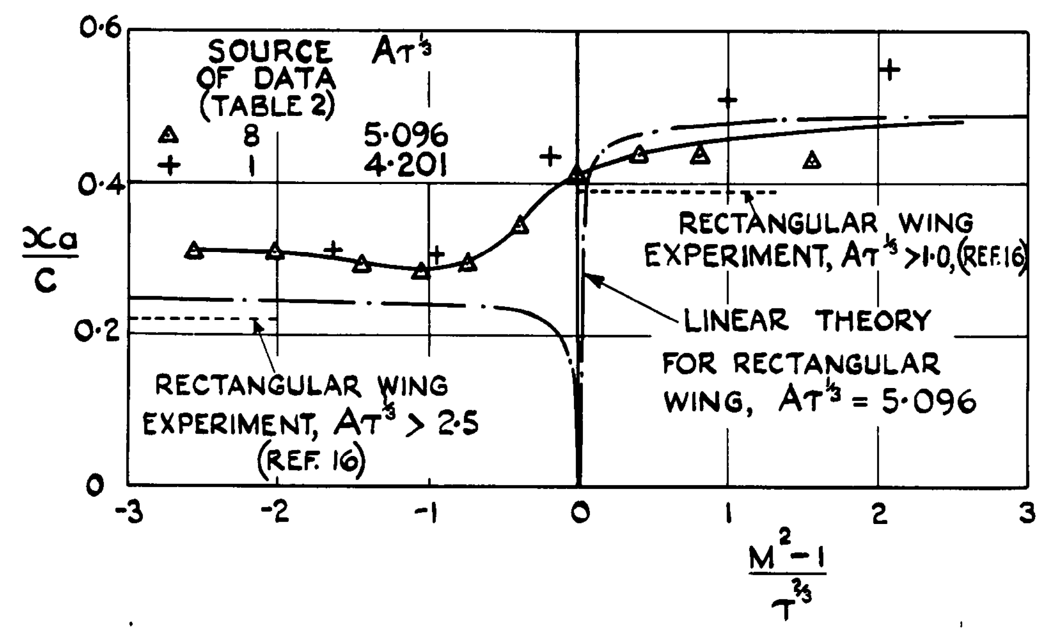

FIG. 18 AERODYNAMIC CENTRE POSITION AT TRANSONIC SPEEDS.

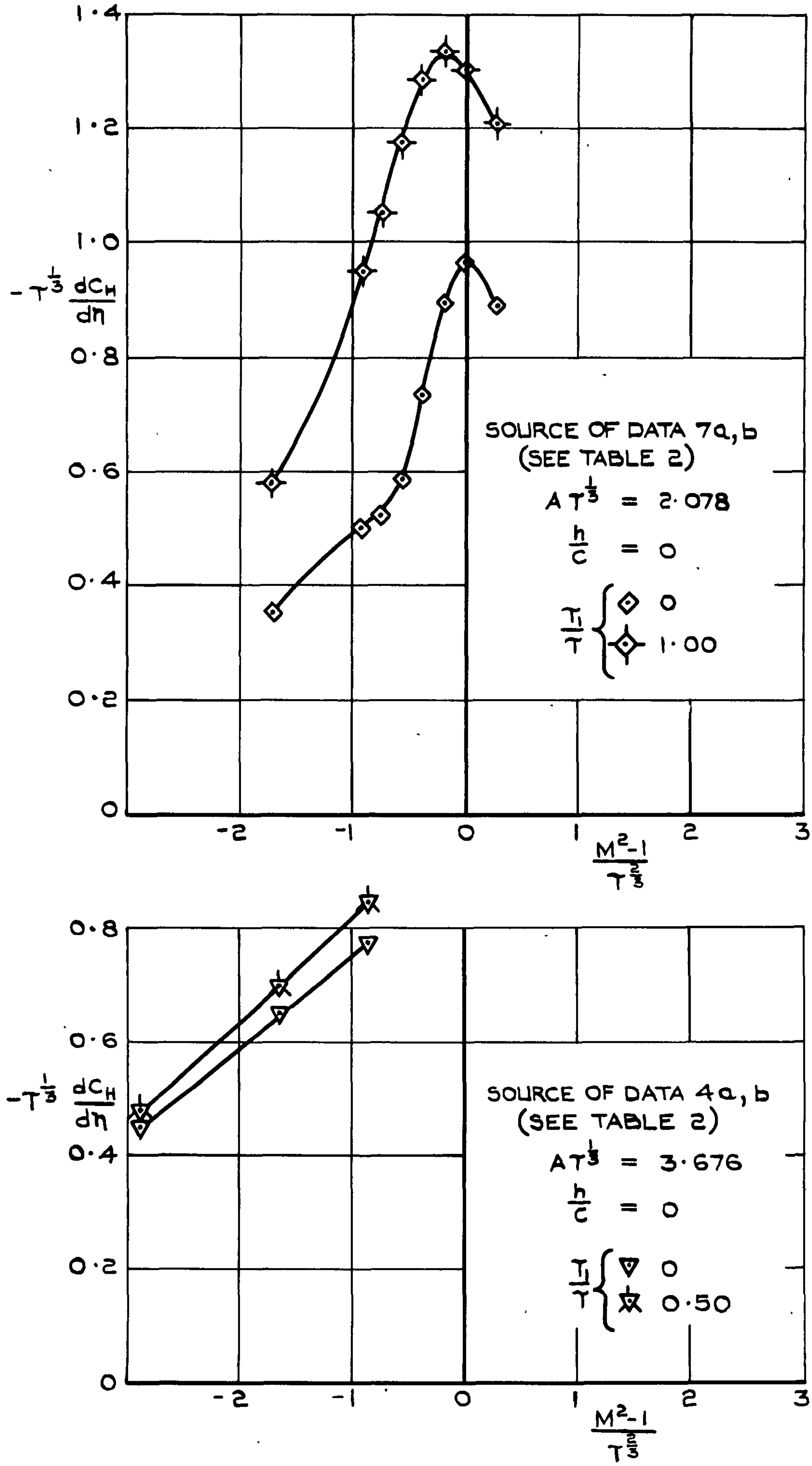

FIG. 19 EFFECT OF TRAILING EDGE THICKNESS ON $\frac{dC_H}{d\eta}$ AT TRANSONIC SPEEDS

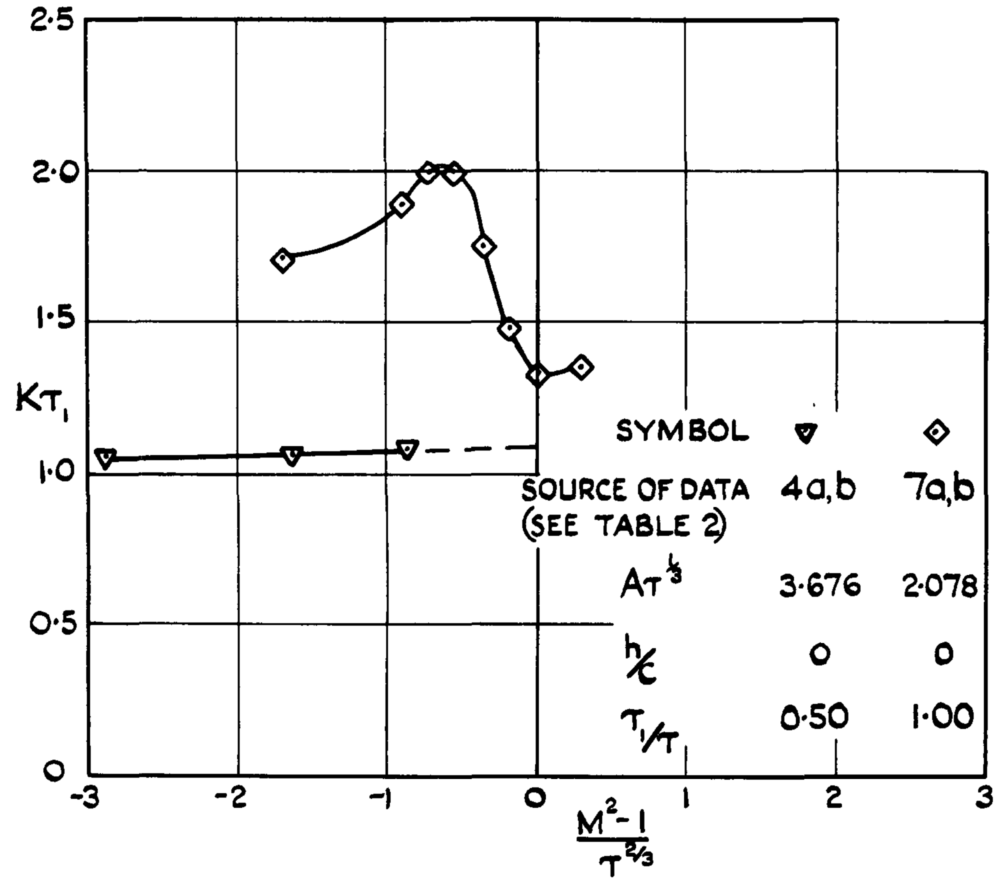

FIG 20 VARIATION OF K_{τ_1} WITH $\frac{M^2-1}{\tau^{2/3}}$ AT TRANSONIC SPEEDS.

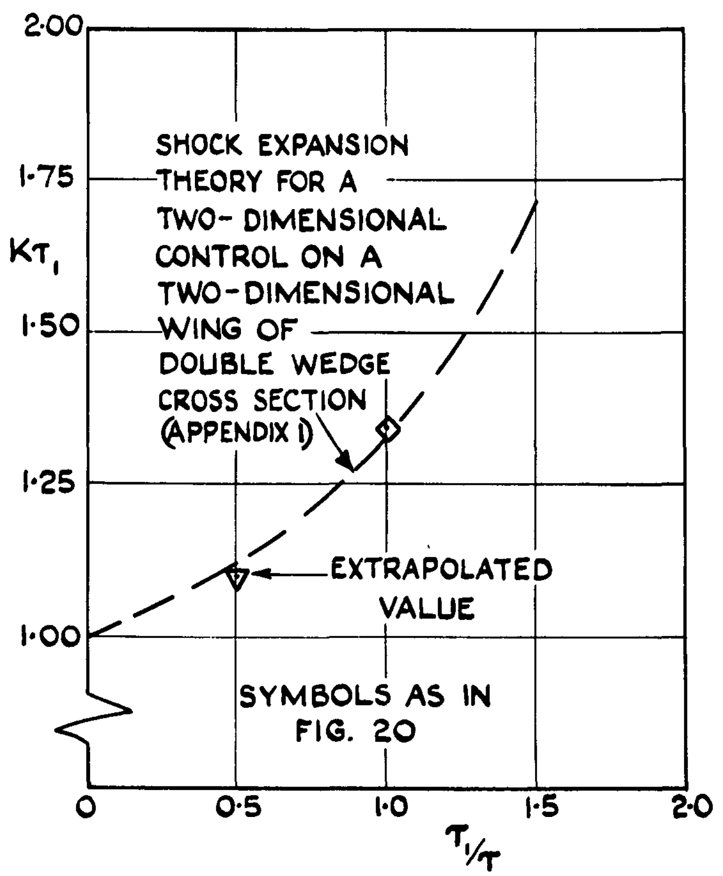

FIG 21 VARIATION OF K_{τ_1} WITH τ_1/τ AT M = 1

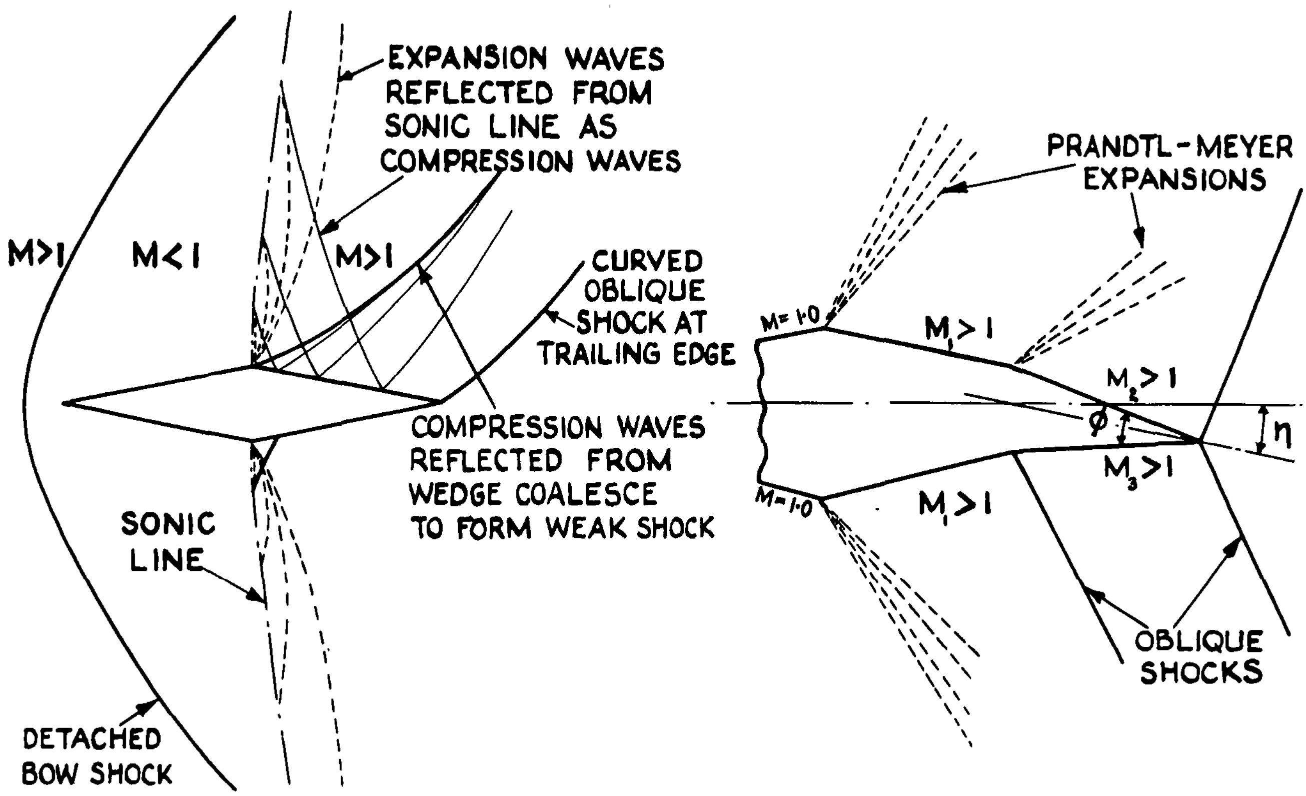

(a) EXACT FLOW MODEL (REF 21) (b) ASSUMED FLOW MODEL

FIG. 22 COMPARISON OF EXACT FLOW PAST DOUBLE-WEDGE PROFILE AT TRANSONIC SPEEDS WITH FLOW MODEL USED IN APPROXIMATE THEORY OF APPENDIX I

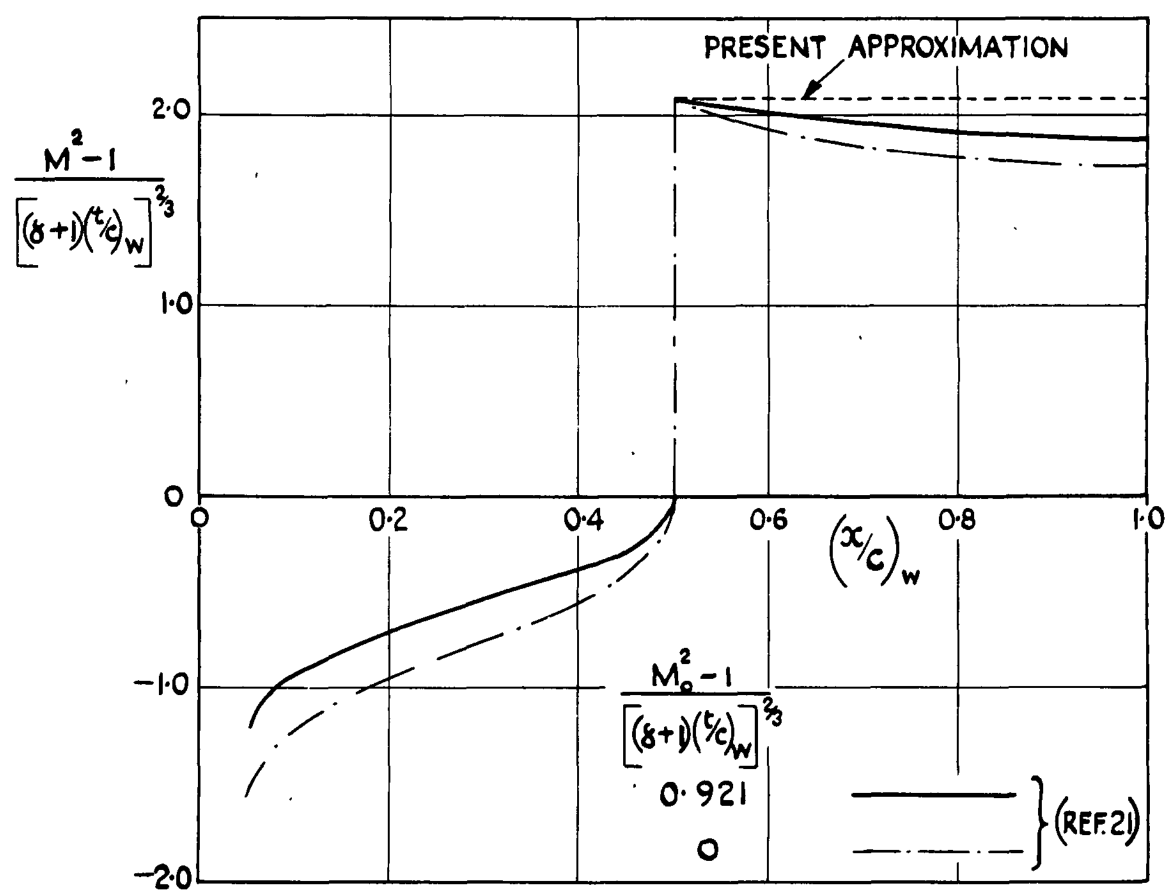

FIG. 23 COMPARISON OF EXACT MACH NUMBER DISTRIBUTION ON DOUBLE-WEDGE PROFILE WITH APPROXIMATION USED IN APPENDIX I.

Printed in England for Her Majesty's Stationery Office by the Royal Aircraft Establishment, Farnborough. Dd.125875. K5.

A.R.C. C.P. No.874

533.694.511 :
533.6.013.155 :
533.6.011.35/5

ANALYSIS OF HINGE MOMENT DATA FOR RECTANGULAR AND NEAR RECTANGULAR TRAILING EDGE CONTROLS AT SUPERSONIC AND TRANSONIC SPEEDS

Isaacs, D.

May 1965

Similarity rules have been used at supersonic and transonic speeds to obtain a correlation of available experimental data on hinge moment curve slope, $(dC_H/d\eta)$, and to compare the experimental values with theoretical estimates.

The effects of varying control aspect ratio, thickness chord ratio, body interference, hinge line location, and trailing edge thickness are examined, suitable theoretical or empirical methods for predicting these effects are indicated, and their range of validity and accuracy determined.

A.R.C. C.P. No.874

533.694.511 :
533.6.013.155 :
533.6.011.35/5

ANALYSIS OF HINGE MOMENT DATA FOR RECTANGULAR AND NEAR RECTANGULAR TRAILING EDGE CONTROLS AT SUPERSONIC AND TRANSONIC SPEEDS

Isaacs, D.

May 1965

Similarity rules have been used at supersonic and transonic speeds to obtain a correlation of available experimental data on hinge moment curve slope, $(dC_H/d\eta)$, and to compare the experimental values with theoretical estimates.

The effects of varying control aspect ratio, thickness chord ratio, body interference, hinge line location, and trailing edge thickness are examined, suitable theoretical or empirical methods for predicting these effects are indicated, and their range of validity and accuracy determined.

A.R.C. C.P. No.874

533.694.511 :
533.6.013.155 :
533.6.011.35/5

ANALYSIS OF HINGE MOMENT DATA FOR RECTANGULAR AND NEAR RECTANGULAR TRAILING EDGE CONTROLS AT SUPERSONIC AND TRANSONIC SPEEDS

Isaacs, D.

May 1965

Similarity rules have been used at supersonic and transonic speeds to obtain a correlation of available experimental data on hinge moment curve slope, $(dC_H/d\eta)$, and to compare the experimental values with theoretical estimates.

The effects of varying control aspect ratio, thickness chord ratio, body interference, hinge line location, and trailing edge thickness are examined, suitable theoretical or empirical methods for predicting these effects are indicated, and their range of validity and accuracy determined.

DETACHABLE ABSTRACT CARDS

C.P. No. 874

© *Crown Copyright 1966*

Published by
HER MAJESTY'S STATIONERY OFFICE

To be purchased from
49 High Holborn, London W.C.1
423 Oxford Street, London W.1
13A Castle Street, Edinburgh 2
109 St. Mary Street, Cardiff
Brazennose Street, Manchester 2
50 Fairfax Street, Bristol 1
35 Smallbrook, Ringway, Birmingham 5
80 Chichester Street, Belfast 1
or through any bookseller

C.P. No. 874

S.O. CODE No. 23-9016-74